Summer 5-20-2011

DNA Photocleavage by 9-Aminomethylanthracene Dyes at pH 7.0: Ionic Strength Effects

Blessing D. Deeyaa
Georgia State University, bdeeyaa1@student.gsu.edu

DNA PHOTOCLEAVAGE BY 9-AMINOMETHYLANTHRACENE DYES AT pH 7.0: IONIC STRENGTH EFFECTS

by

BLESSING D. DEEYAA

Under the Direction of Dr. Kathryn B. Grant

ABSTRACT

DNA photosensitizers are compounds that are capable of binding in to DNA strands through groove binding, intercalation, or electrostatic interactions. Excitation of these agents by light generates reactive oxygen species which causes extensive photo-oxidative damage to genomic DNA. Physiological concentrations of NaCl and KCl are ~ 150 mM and 260 mM within the cell nucleus where DNA is contained. Unfortunately, the ability of most photosensitizers to bind to double-helical DNA is reduced and photocleavage yields are diminished as concentrations of salt increase. The aim of this project is to observe the photocleavage of pUC19 plasmid DNA induced by N^1,N^1-bis(9-anthrymethyl)triethylenetetraamine tetrahydrochloride (AL-VIII 23) **1** or *N,N*-dimethyl-*N'*-(9-methylanthracenyl)ethylenediamine (NMEA) **2** in presence of salt. Spectroscopic titrations and DNA melting assays were used to study binding modes and affinities of both dyes to the helix upon the addition of salt.

INDEX WORDS: Photocleavage, Anthracene, Intercalators, Groove binders

DNA PHOTOCLEAVAGE BY 9-AMINOMETHYLANTHRACENE DYES AT pH 7.0: IONIC STRENGTH EFFECTS

by

BLESSING D. DEEYAA

A Thesis Submitted in Partial Fulfillment of the Requirement for the Degree of Master of Science

In the College of Arts and Sciences

Georgia State University

2011

DNA PHOTOCLEAVAGE BY 9-AMINOMETHYLANTHRACENE DYES AT pH 7.0: IONIC STRENGTH EFFECTS

by

BLESSING D. DEEYAA

Committee Chair: Dr. Kathryn B. Grant

Committee: Dr. Dabney W. Dixon
Dr. Donald Hamelberg

Electronic Version Approved:

Office of Graduate Studies
College of Arts and Science
Georgia State University
May 2011

ACKNOWLEDGEMENTS

First off, I would like to acknowledge my advisor, Dr. Kathryn Grant for taking me in as an undergraduate student and molding me into the scientist I have become. She always motivated me and was optimistic even when my experimental results were unexpected. Thank you for all you support and teaching me to always reach for the best.

I would also like to acknowledge my undergraduate chemistry professor Dr. Devon Kennedy. Thank you for all the wonderful advice you gave me throughout my time here at GSU and also for teaching me the importance of time management and developing healthy study habits. I would like to thank Lanette Brown for being my GSU fairy godmother and always coming to my rescue whenever I needed help. I would also like to thank Dr. Sarah Stoll for giving my first research opportunity as an undergraduate student.

I would also like to acknowledge my lab members Carla Terry, Dominique Williams, Sarah Green, and Rashida Payne for all their support and guidance. Thank you Carla for being my graduate mentor and always pointing me in the right direction whenever I needed help. Thanks Dominique and Rashida for being such helpful and supportive friends both in and out of the lab. Power to the girls, I love you guys and I am truly going to miss every single member of the Grant lab.

Last but not least, I would like to thank my committee members, Dr. Dixon and Dr. Hamelberg for accepting the position despite their busy schedules and my time constraints. Thank you both for looking out for my best interests.

TABLE OF CONTENTS

LIST OF TABLES

LIST OF FIGURES

LIST OF SCHEMES

1. Introduction

1.1 Brief Overview of Photodynamic Therapy

Photodynamic therapy (PDT) is a clinical procedure that involves the administration of a photosensitizer to a target cell to induce necrosis or apoptosis [1]. This procedure is used mostly for treatment of superficial lesions of malignant and non-malignant diseases. The process involves the administration of small quantities of a photosensitizing drug and irradiation of the target tissue with visible light (~500 - 800 nm). A photosensitizer is a compound that produces reactive oxygen species (ROS) when excited by a photon of light of a specific wavelength. The generation of these ROS leads to a series of photochemical reactions that consequently lead to DNA damage thereby inhibiting transcription and cell replication. Factors that contribute to cell damage include the location and concentration of photosensitizer administered [2]. Since the discovery of photodynamic therapy as a treatment for cancerous tumors, the need to discover new and efficient photosensitizers has grown tremendously.

Phototherapy has been applied by humans to treat various diseases for over 3000 years. Ancient Greek civilizations (~ 2nd century B.C.) believed heliotherapy was the healing ability of the sun to restore human health [3]. The term 'photodynamic action' originated from Professor Herman von Tappeiner, director of Pharmacology Institute of Ludwig-Maximilians University in Munich in 1904. He attempted the use of several dyes for PDT treatment of tumors and skin diseases such as lupus chondylomata [3]. In 1903, a Nobel Prize in Medicine was awarded to Niels Finsen for his work in phototherapy, using carbon arc for treatment of lupus vulgaris [4]. In 1943, Auler and Banzer reported the use of a porphyrin derivative haematoporphyrin (Figure 1.1) as a photosensitizer to treat tumor cells. They reported that the compound showed a high affinity for primary and metastatic tumor cells than healthy cells [5, 6]. As research progressed

in this field, Lipson *et al*. designed a haematoporphrin derivative (HpD) that had a higher affinity and phototoxicity for cancer cells [7]. This derivative became the first synthetic compound used in photo treatment of cancerous tumor [6]. Through further purification of HpD, Thomas Doughery and his colleagues at Roswell Park Memorial Cancer Institute developed Photofrin I (Figure 1.2) [8]. It was the first FDA approved drug used for PDT. Upon irradiation with red-light, Photofrin I was capable of inhibiting tumor growth in humans but its applications were limited to treatment of near surface tumors [3, 6]. Subsequently, drugs such as Levulan, Metvis, Foscan, and Laserphyrin were also approved for clinical use [3].

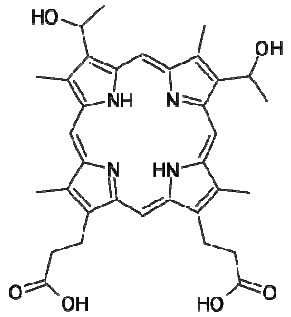

Figure 1.1: Structure of hematoporphyrin.

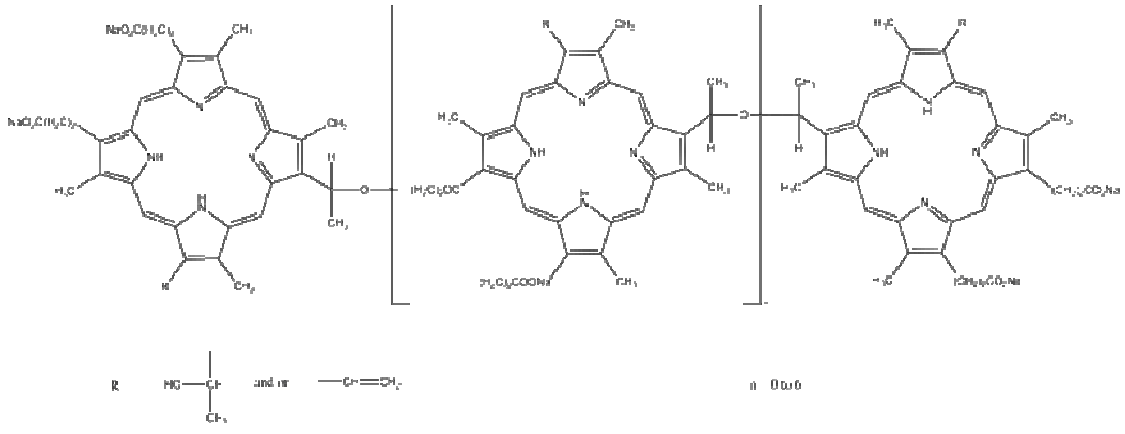

Figure 1.2: A component of Photofrin 1, the first FDA approved drug used for photodynamic therapy. Image was reproduced from reference [9].

1.2 Photo-excitation of Photosentizers

Photosensitizing compounds usually possess conjugated π ring systems. Most photosensitizers have fluorescence emission spectra that overlap with their absorption spectra. Some of them show strong absorbance in the red region of the spectrum [2]. Most scientists agree that the qualities of an ideal photosensitizer would include a high extinction coefficient, high quantum yield of singlet oxygen, low dark toxicity, long absorbing wavelength, and rapid removal from the body [10]. The compounds are administered either topically or by injecting the photosensitizer into the blood stream and exposing the target tissue to light once the photosensitizer is localized in the target cell [11]. Most photosensitizers tend to bind to tumor cells with greater affinity than normal cells and it is necessary to wait for the compound to be flushed out of the normal cells before activation and production of cytotoxic species [10].

Photosensitizers are capable of causing DNA damage through Type I and Type II oxidative pathways (Figure 1.3). When a photosensitizer is exposed to light, a singlet state (^1P) is produced by absorption of electromagnetic radiation. The singlet state can then undergo intersystem crossing to produce a triplet state [12]. Type 1 reactions involve a direct transfer of an electron to the molecular oxygen or from DNA nucleobases, preferentially guanine to the excited state photosensitizer, leading to the generation of superoxide ion radicals ($O_2^{\bullet-}$) and DNA base oxidation. The oxidation of guanine typically leads to the formation of 7,8-dihydro-8-oxoguanine (8-oxoG). The formation of superoxide anions leads to the production of hydroxyl radicals ($^{\bullet}OH$), generated via the Fenton reaction [13]. The presence of hydroxyl radicals leads to the abstraction of hydrogen atoms from the deoxyribose sugar, forming alkali-labile lesions and direct strand cleavage. Hydroxyl radicals can also cause direct oxidation of DNA bases, preferentially C-8 of guanine, leading again to the formation of 8-oxoG. In Type II reactions,

energy is transferred from the excited triplet state of the photosensitizer to the triplet ground state of molecular oxygen, leading to the formation singlet oxygen which preferentially oxidizes guanine [13-16]. Both pathways are toxic to the cell and can induce necrosis or apoptosis of living tissue.

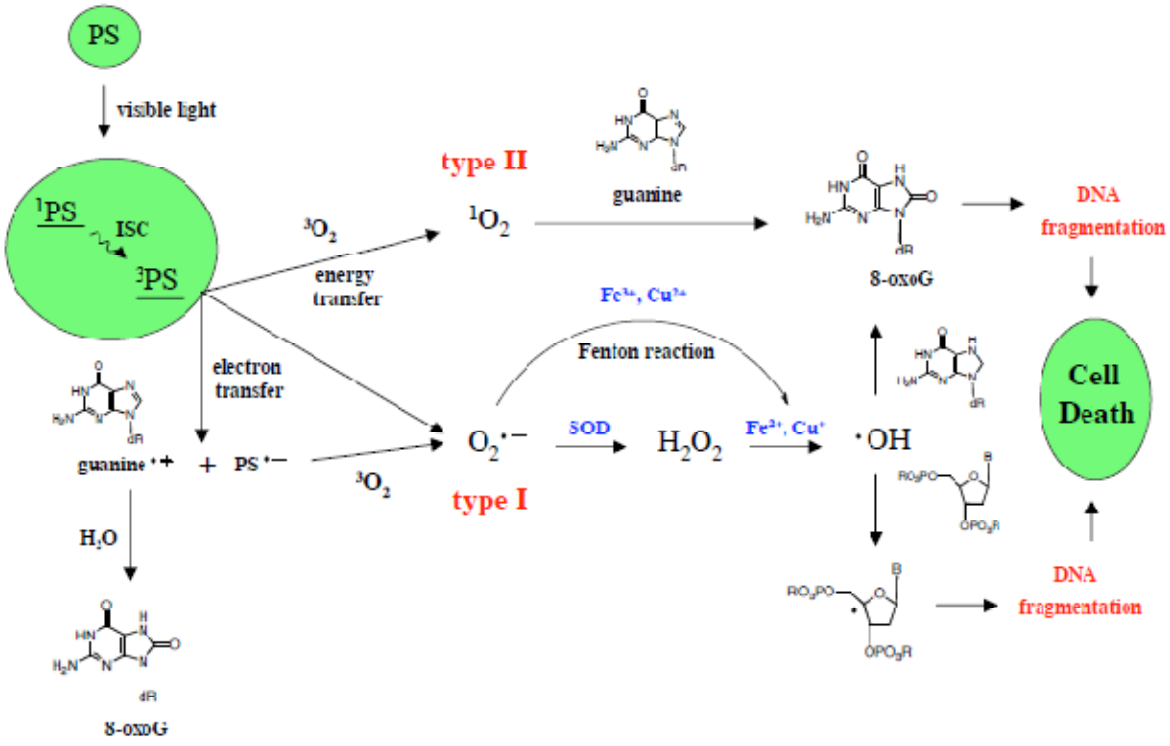

Figure 1.3: Scheme of DNA damage by photosensitizer reproduced from reference [12].

1.3 Non-covalent Interactions with DNA

Photosensitizers interact with DNA through three possible binding modes: electrostatic external interactions, groove binding, and intercalation (Figure 1.4) [1]. These various modes of binding have different effects on DNA conformation and initiation of photoreactions. This thesis will focus on groove binding and intercalation modes of interaction.

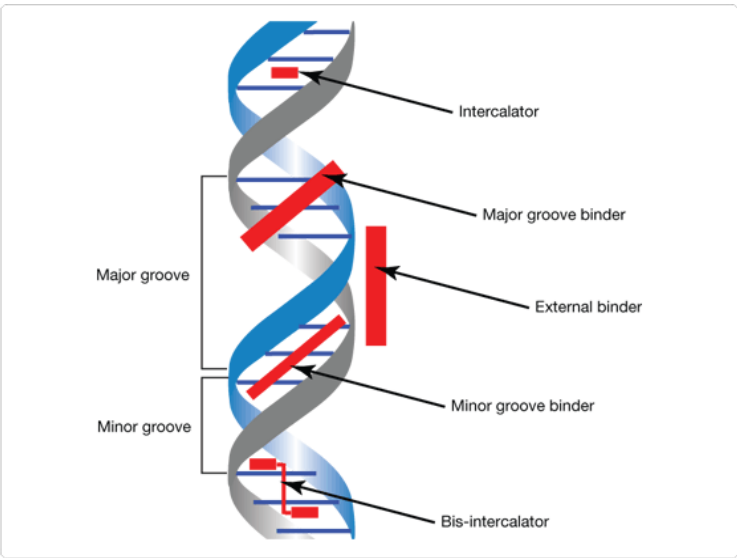

Figure 1.4: Non-covalent DNA binding modes reproduced from reference [17].

1.3.1 Groove Binding Compounds

DNA groove binders interact with either the major or minor grooves of the helix. Large molecules like proteins tend to bind primarily to the major groove while smaller molecules prefer the minor groove of DNA [18]. The smaller molecules are usually composed of small aromatic rings such as pyrroles, furans, and benzenes linked by amide groups. They may also possess crescent shapes with appropriate twist to fit into the curve of the minor groove. When the compound is fitted properly into the minor groove, water molecules are displaced from the groove and the compound forms van der Waals contacts with the groove walls [18]. Groove binder molecules show some sequence specificity with a majority showing hydrogen bonding preference to A-T rich sequences [19]. The amino group hydrogen of the amide bond between the aromatic rings are capable of hydrogen bonding to the C-2 carbonyl oxygen of thymine or N-3 nitrogen of adenine. A similar interaction with guanine and cytosine bases is unlikely due to the added steric bulk of the G-NH_2 [18].

1.3.2 Intercalating Compounds

Intercalators are molecules that bind to DNA by insertion between the base pairs. Intercalators can be grouped into mono, bis, and threading intercalators. Most intercalators are planar molecules containing fused aromatic rings with a charged side chain attached to the ring. The planarity of the ring system favors stacking with the DNA base pairs [20]. As the compound binds between the bases, the helix conformation is altered [21]. There is a localized unwinding of helix and an increase in the helical rise as the compound binds. The unwinding and lengthening of the DNA strands causes and increase in the viscosity of the solution [22].

Most intercalators abide by the nearest neighbor exclusion principle when they bind to DNA [23]. This principle is based on the theory that most intercalators bind between every other DNA base pair to reach saturation. The flexibility of the linker also plays a major role in the ability of the compound to intercalate. Polyamine linkers such as spermine bind across the major groove of B-form DNA and interact with the negatively charged phosphate groups. Polyamines are usually protonated under physiological conditions. Based on its net charge, a linker might be capable of forming salt bridges with the phosphate back bone [1].

Scientists have synthesized bis-intercalators with varying lengths of linkers to test the effects on the linker length on intercalation position [23]. A bis-intercalator is a compound that contains two polycylic aromatic hydrocarbons connected by a linker (Figure 1.5). They are capable of binding simultaneously to two sets of DNA base pairs. By shortening or lengthening its linker, the distance of the intercalation can be somewhat controlled [23]. Some examples of bis-intercalators include ditercalinium, echinomycin, and triostin A [18, 24].

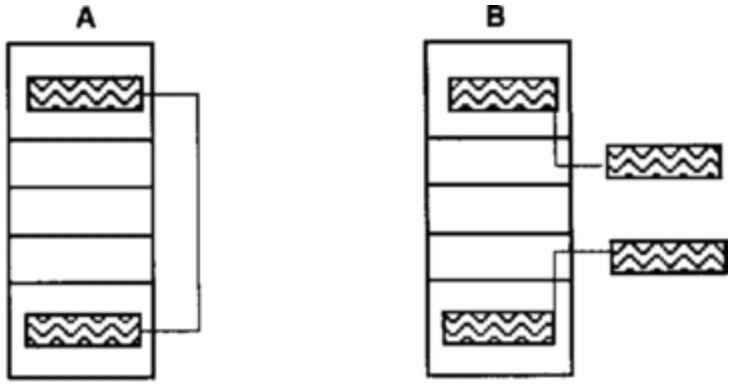

Figure 1.5: Image of possible conformations of a bis-intercalator reproduced from reference [25].

1.4 Anthracene Based DNA Interactions

Anthracenes are made up of three planar fused aromatic rings. They fall under the category of fluorescent dye photosensitizers. They are capable of light dependent chemical reactions that result in damage of biological systems. Anthracenes are good photosensitizers because of their low polarizability, strong fluorescence, good absorption in the near UV region, and a long-lived excited triplet state [26]. They are capable of producing ROS through either type I and type II reaction pathways. Anthracenes produce singlet oxygen by energy transfer from their singlet and triplet excited states when irradiated with light [20, 27]. Mechanisms of cleavage include hydrogen abstraction from the sugar ring by photochemically generated radicals, direct electron transfer from the base (usually guanine) to the excited photosensitizer, singlet oxygen production by transfer of energy from the excited photosensitizer, and formation of base adducts with the photosensitizer. The production of radicals and reactive oxygen species produces extensive phototoxic damage to DNA by forming alkaline labile lesions and direct strand breaks at guanine bases [14].

The cleavage of DNA is important because it could lead to apoptosis or necrosis of the cells. When anthracene based photosensitizers are introduced to tissue they are known to

possess anti-tumor and anti-viral activity. When linked to a primary alkyl amine, they can undergo photochemical reactions with nucleotides that induce DNA strand scission [20]. The two major bind modes of anthracene chromophores are intercalation and groove binding. Large substituents on the anthracene ring are known to inhibit intercalation due to steric clash with the amino group of guanine in the minor groove [26]. These compounds bind to the DNA through either the major or minor grooves. Based on the structure and net charge of the compound, it could also form electrostatic interactions with the phosphate backbone or be a threading intercalator.

One of the many challenges of designing new anthracene-based photosensitizers is determining its binding mode and affinity to DNA. Several anthracenes are known to intercalate between DNA base pairs [20, 26]. Most intercalators show preferential binding to alternating purine-pyrimidine sequences [20]. Spectroscopic characteristics of intercalation include strong hyprochromism, red shifts in vibronic bands, lengthening of excited state lifetime, induced circular dichorism, and increased stability of the DNA helix. Observed large hypochromism suggests that the anthryl chromophore is in close proximity to the bases [20]. There are several methods of evaluating anthryl binding mode including UV-visible titrations, DNA melting studies, ^{1}H and ^{31}P NMR, and isothermal calorimetry, as well as linear and circular dichroism studies [26, 28]. Based on spectroscopic data, the binding affinity of the anthryl chromophore can be determined.

Several anthracyclines and anthracenediones have been approved by the FDA for treatment of diseases such as lung cancer, breast cancer, lymphoid and myeloid leukemia. Examples of such compounds include daunorubicin, dactinomycin, mitoxantrone, and doxorubicin [29]. These anthryl chromophores are photosensitive compounds, yielding high

cytotoxicity and inducing double strand DNA breaks when activated by light. They are also known to bind to DNA through intercalation [30].

1.5 Goal

This research focuses on the study of anthracene chromophores with respect to their ability to induce DNA damage for future use in PDT. These compounds are expected to bind to DNA via intercalation or groove binding and induce photocleavage when irradiated by light. Previous research done by the Grant and Lorente groups showed that anthracene chromophores are capable of binding to DNA via groove binding or intercalation and inducing cleavage of the helix when activated by UV light. Spectroscopic studies showed that there is a change in anthracene binding mode when 150 mM of NaCl and 260 mM KCl are added to the reaction [31]. Under conditions of increased ionic strength, phosphate-phosphate repulsion is decreased. This results in the decreased groove binding and intercalation and also contraction of the helix [32].

The compounds shown below were capable of inducing cleavage to double stranded DNA when activated by 350 nm light. Photocleavage reactions were performed using pUC19 plasmid DNA isolated from the bacterium *E. coli*. This plasmid DNA is a double stranded, circular supercoiled accessory chromosome containing 2686 base pairs. It is commonly used in DNA related experiments because it has a high copy number, is inexpensive, relatively small in size, and readily available. The photocleavage experiments were conducted with the aim of mimicking physiological conditions within the cell nucleus using 10 mM phosphate buffer (pH 7.0), 150 mM NaCl and 260 mM KCl [33 – 35]. Studies have shown that the presence of salt decreases the binding affinity of photosensitizers to DNA helix thereby reducing photocleavage yields [21, 32]. Photocleavage studies were done to evaluate the extent of DNA damage when

these compounds were irradiated by 350 nm light. UV-visible and DNA melting studies were also done to evaluate binding modes of the ligand to the DNA.

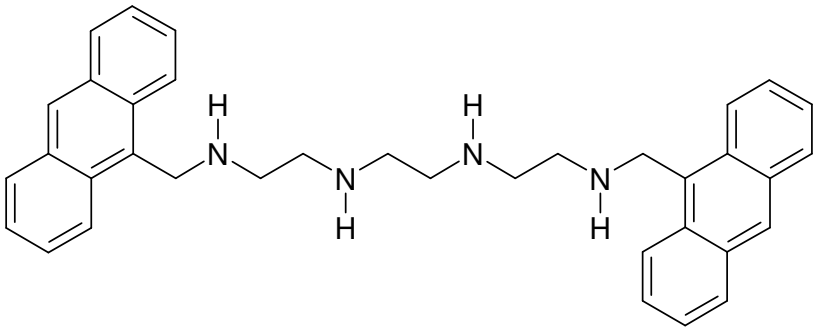

N^{1},*N*^{1}-bis(9-anthrymethyl)triethylenetetraamine 4 HCl (AL-VIII 23) (**1**)

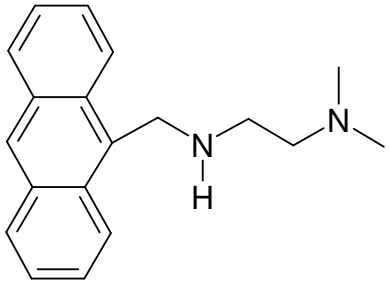

N,N-dimethyl-*N'*-(9-methylanthracenyl)ethylenediamine (NMEA) (**2**)

2 Experimental

2.1 General Methods

Sodium chloride was purchased from EMD Chemical Inc (Gibbstown, NJ). Agarose, 9-anthraldehyde, potassium chloride, *N,N*-dimethylethylendiamine, bromophenol blue, and Ficoll type 400 were purchased from Sigma Aldrich (St. Louis, MO). Tris base and monobasic sodium phosphate were from Fisher Scientific (Fairlawn, NJ). Xylene cyanol FF was purchased from Eastman Kodak (Rochester, NY). UltraPure ^{TM} calf thymus DNA solution ~ 2000 bp was from Invitrogen (Carlsbad, CA). DNA concentration was quantitated using Beer's Law with an extinction coefficient of 12,824 M^{-1} (bp) cm^{-1} at 260 nm. The pUC19 plasmid was cloned by Carla Terry (Georgia State University) according the procedures described in the literature [36].

Samples were weighed on an analytical balance (Mettler Toledo B154, Switzerland). Photocleavage of pUC19 DNA was carried out using twelve 350 nm light bulbs (12 inches) in a Rayonet Photochemical Reactor (Model PRP-100, Southern New England Ultra Violet Company, Branford, CT). Gel electrophoresis was carried out using an Owl horizontal electrophoresis system (ThermoScientific, Rochester, NY) attached to a VWR 105 Voltmeter (VWR Scientific, E-C Apparatus). Gel images were captured using a Canon Powershot A640 digital camera. UV-visible experiments were carried out on a Shimadzu UV-1601 spectrophotometer (Shimadzu Scientific Instruments Inc, Japan). Thermal melting studies were conducted on a Cary Win Spectrophotometer (Varian Inc.). Mass spectrometry analysis was conducted on a Water Q-TOFmicro, ABI API 3200 triple quadrupole ESI instrument and ^{1}H NMR analysis was carried out on a Bruker Avance 400 NMR spectrometer.

2.2 Synthesis of *N,N*-dimethyl-*N'*-(9-methylanthracenyl)ethylenediamine

Compound **2** was synthesis according to procedures described by Bag and Bharadwaj shown in Scheme 1 [37]. A solution of 9-anthraldehyde (1.2405g; 6.00 mmol) and ethanol (70 mL) was added to *N,N*-dimethylethylenediamine (0.70 mL; 6.00 mmol) and allowed to stir at room temperature for 36 h. Excess $NaBH_4$ (0.2765g) was added to the solution which was heated to reflux for 4 h. The reaction was monitored using aluminum thin layer chromatography (TLC) sheets (silica gel 60, EMD, Germany). The solvent was removed under reduced pressure. The resulting yellow solid was stirred in 100 mL of water for 30 min and extracted with 40 mL dichloromethane. The organic layer was dried over anhydrous $MgSO_4$. The remaining solvent was evaporated to dryness and a brown semi-solid product **2** was obtained (83% yield). ^1H NMR (400 MHz, $CDCl_3$, 25°C) 2.17 (s, 6H), 2.49 (s, 2H), 4.73 (s, 2H), 5.23 (s, 1H), 7.44 (t, 2H), 7.52 (t, 2H), 7.52 (t, 2H), 7.88 (d, 2H), 8.42 (m, 3H). ESI-MS (m/z) Anal. Calcd for $C_{19}H_{23}N_2$: $[M+H]^+$ 279.1861, found: 279.1856.

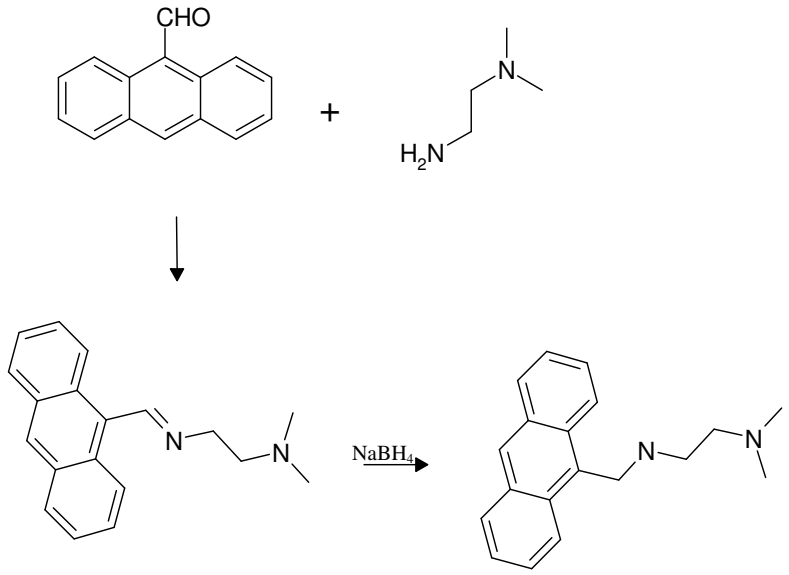

Scheme 1: Synthesis of *N,N*-dimethyl-*N'*-(9-methylanthracenyl)ethylenediamine

2.3 Preparation of Stock Solutions

2.3.1 Preparation of ALVIII-23

N^1,N^1-Bis(9-anthrymethyl)triethylenetramine tetrahydrochloride (**1**) was synthesized by Prof. Antonio Lorente at Universidad de Alcalá, Spain. Photocleavage samples were prepared by dissolving 0.0034 g of ALVIII-23 (F.W.= 672.55 g/mol) in 1.00 ml DMSO to make a 5 mM solution. Samples were then diluted into ten 100 μM aliquots and stored in a freezer at -20 ^{o}C.

2.3.2 Preparation of NMEA

Compound **2** was prepared by dissolving 0.00143 g of 9-NMEA (F.W.= 285.82 g/mol) in 1 ml DMSO to make a 5 mM solution. Samples were then diluted into ten 100 μM aliquots and stored in a freezer at -20 ^{o}C.

2.3.3 Preparation of NaCl and KCl

Stock solutions of 1.0 M NaCl was prepared by dissolving 5.84 g NaCl (100 mmol) in 100 mL autoclaved deionized water (ddH_2O). Potassium chloride stock solution was preparing similarly by dissolving 7.46 g KCl (100 mmol) in 100 mL ddH_2O.

2.3.4 Preparation of Sodium Phosphate Buffer

Buffer made by preparing 1.0 M solutions of mono and dibasic sodium phosphate. To prepare the monobasic salt, 35.49 g NaH_2PO_4 was dissolved in 250 mL ddH_2O. The same amount of dibasic salt was also dissolved in 250 mL ddH_2O. Both monobasic and dibasic sodium phosphate solutions were diluted in ddH_2O to a total volume of 1000 mL by combining 57.7 mL of NaH_2PO_4 and 42.3 mL of Na_2HPO_4. The pH was adjusted to 7.0 using 50% NaOH (19 M, Fisher Scientific).

2.3.5 Preperation of Tris Acetate EDTA Buffer

A 50X buffer solution was prepared by diluting 242 g Tris base, 57.1 mL glacial acetic acid, 100 mL of 0.5 M EDTA (pH 8.0) to a total volume of 1000 mL. The buffer was then diluted to a 1X concentration using the equation below:

$$M_1V_1 = M_2V_2$$

2.4 Preparation of Photocleavage Samples

2.4.1 Concentration Titrations with NaCl

Photocleavage samples were prepared following the volumes listed in Tables 2.1 and 2.2 for a total of 40 μL each. The solutions were added to Eppendorf tubes in the order listed below.

ddH_2O
100 mM Sodium phosphate buffer (pH 7)
300 ng/μL pUC19
100 μM or 10 μM Dye
1 M NaCl

Samples were prepared with increasing concentrations of dye (0-10 μM) in the presence and absence of 150 or 260 mM NaCl and allowed to equilibrate in the dark for 60 min. For the 1.0 and 0.5 μM dye concentrations the 100 μM stock solution was diluted to 10 μM in ddH_2O. They were then aerobically irradiated for 60 min in a Rayonet Photochemical reactor fitted with twelve 350 nm lamps. Negative controls remained in the dark while the photocleavage reaction proceeded.

Table 2.1: Photocleavage with addition 150 mM NaCl

Units in μL (Total Volume 40 μL)															
[Stock]	[Working]	1	2	3	4	5	6	7	8	9	10	11	12	13	14
Dye Concentration (μM)		10	5	2.5	1	0.5	0	10	10	5	2.5	1	0.5	0	10
pUC19 (300 ng/μL)	pUC19 (15 ng/μL)	2	2	2	2	2	2	2	2	2	2	2	2	2	2
Dye (100 μM)	Dye (10 μM – 0 μM)	4	2	1	0.4	0.2	0	4	4	2	1	0.4	0.2	0	4
Phos Buffer (100 mM)	Phos Buffer (10 mM)	4	4	4	4	4	4	4	4	4	4	4	4	4	4
NaCl (1.0 M)	NaCl (150 mM)	6	6	6	6	6	6	6	~	~	~	~	~	~	~
	ddH_2O	24	26	27	27.6	27.8	28	24	30	32	33	33.6	33.8	34	30
	Light (60 min)	(+)	(+)	(+)	(+)	(+)	(+)	(--)	(+)	(+)	(+)	(+)	(+)	(+)	(--)

Table 2.2: Photocleavage of addition of 260 mM NaCl

Units in μL (Total Volume 40 μL)															
[Stock]	[Working]	1	2	3	4	5	6	7	8	9	10	11	12	13	14
Dye Concentration (μM)		10	5	2.5	1	0.5	0	10	10	5	2.5	1	0.5	0	10
pUC19 (300 ng/μL)	pUC19 (15 ng/μL)	2	2	2	2	2	2	2	2	2	2	2	2	2	2
Dye (100 μM)	Dye (10 μM – 0 μM)	4	2	1	0.4	0.2	0	4	4	2	1	0.4	0.2	0	4
Phos Buffer (100 mM)	Phos Buffer (10 mM)	4	4	4	4	4	4	4	4	4	4	4	4	4	4
NaCl (1.0 M)	NaCl (260 mM)	10.4	10.4	10.4	10.4	10.4	10.4	10.4	~	~	~	~	~	~	~
	ddH_20	19.6	21.6	22.6	23.2	23.4	23.6	19.6	30	32	33	33.6	33.8	34	30
	Light (60 min)	(+)	(+)	(+)	(+)	(+)	(+)	(--)	(+)	(+)	(+)	(+)	(+)	(+)	(--)

2.4.2 Concentration Titration with KCl

The samples were prepared by combining the following stock solutions into an Eppendorf tube and equilibrating in the dark for 60 min.

ddH_2O
100 mM Sodium phosphate buffer (pH 7)
300 ng/μL pUC19
100 μM or 10 μM Dye
1 M KCl

The mixture was then placed in a Rayonet Photoreactor and aerobically (air) irradiated for 60 min at 350 nm. For the 1.0 and 0.5 μM dye concentrations the 100 μM stock solution was diluted to 10 μM in ddH_2O. Samples 7 and 14 from Table 2.3. remained in the dark while the others were being irradiated. After 1 h elapsed, the samples were removed from the photoreactor and 3 μL of loading buffer (0.25% xylene cyanol FF, 0.25% bromophenol blue, 15% Ficoll Type 400) was added to each tube for gel electrophoresis.

Table 2.3: Photocleavage with addition 260 mM KCl

Units in μL (Total Volume 40 μL)															
[Stock]	[Working]	1	2	3	4	5	6	7	8	9	10	11	12	13	14
Dye Concentration (μM)		10	5	2.5	1	0.5	0	10	10	5	2.5	1	0.5	0	10
pUC19 (300 ng/μL)	pUC19 (15 ng/μL)	2	2	2	2	2	2	2	2	2	2	2	2	2	2
Dye (100 μM)	Dye (10 μM – 0 μM)	4	2	1	0.4	0.2	0	4	4	2	1	0.4	0.2	0	4
Phos Buffer (100 mM)	Phos Buffer (10 mM)	4	4	4	4	4	4	4	4	4	4	4	4	4	4
KCl (1.0 M)	KCl (260 mM)	10.4	10.4	10.4	10.4	10.4	10.4	10.4	~	~	~	~	~	~	~
	ddH_20	19.6	21.6	22.6	23.2	23.4	23.6	19.6	30	32	33	33.6	33.8	34	30
	Light (60 min)	(+)	(+)	(+)	(+)	(+)	(+)	(--)	(+)	(+)	(+)	(+)	(+)	(+)	(--)

2.4.3 Concentration Titration with NaCl and KCl

Photocleavage samples were prepared following the volumes listed in Table 1 and 2 at a total of 40 μL each. The solutions were added to Eppendorf tubes in the order listed below.

ddH_2O
100 mM Sodium phosphate buffer (pH 7)
300 ng/μL pUC19
100 μM or 10 μM Dye
1 M NaCl

Individual samples containing increasing concentrations of dye (0-10 μM) in the presence or absence of 150 or 260 mM NaCl were allowed to equilibrate in the dark at room temperature for 60 min. For the 1.0 and 0.5 μM dye concentrations the 100 μM stock solution was diluted to 10 μM in ddH_2O. They were then aerobically irradiated for 60 min in a Rayonet Photochemical reactor. Negative controls remained in the dark while the photocleavage reaction proceeded. Once the reaction time had elapsed, the samples were removed from the photoreactor and 3 μL of loading buffer was added to each tube and mixed homogenously.

Table 2.4: Photocleavage with addition 150 mM NaCl and 260 mM KCl

Units in mL (Total Volume 40 μL)															
[Stock]	[Working]	1	2	3	4	5	6	7	8	9	10	11	12	13	14
Dye Concentration (μM)		10	5	2.5	1	0.5	0	10	10	5	2.5	1	0.5	0	10
pUC19 (300 ng/μL)	pUC19 (15 ng/μL)	2	2	2	2	2	2	2	2	2	2	2	2	2	2
AL- VIII (100 μM)	AL-VIII (10 μM – 0 μM)	4	2	1	0.4	0.2	0	4	4	2	1	0.4	0.2	0	4
Phos Buffer (100 mM)	Phos Buffer (10 mM)	4	4	4	4	4	4	4	4	4	4	4	4	4	4
NaCl (1 M)	NaCl (150 mM)	6	6	6	6	6	6	6	~	~	~	~	~	~	~
KCl (1.0 M)	KCl (260 mM)	10.4	10.4	10.4	10.4	10.4	10.4	10.4	~	~	~	~	~	~	~
	ddH_20	13.6	15.6	16.6	17.2	17.4	17.6	13.6	30	32	33	33.6	33.8	34	30
	Light (60 min)	(+)	(+)	(+)	(+)	(+)	(+)	(--)	(+)	(+)	(+)	(+)	(+)	(+)	(--)

2.4.4 Time Course Titration with NaCl and KCl

Samples were prepared according to the order listed in Table 2.5 by adding the following solutions to an Eppendorf tube.

ddH_2O
100 mM Sodium phosphate buffer (pH 7)
300 ng/μL pUC19
100 μM Dye
1 M NaCl
1 M KCl

The samples were allowed to equilibrate in the dark for 1 h and aerobically (air) irradiated for 0-60 min in a Rayonet Photochemical reactor. After the tubes were removed from the photo reactor, 3 μL of loading buffer was added to each solution and mixed homogenously.

Table 2.5: Time course titration

Units in μL (Total Volume 40 μL)															
[Stock]	[Working]	1	2	3	4	5	6	7	8	9	10	11	12	13	14
AL- VIII Concentration (μM)		2.5	2.5	2.5	2.5	2.5	2.5	2.5	2.5	2.5	2.5	2.5	2.5	2.5	2.5
pUC19 (300 ng/μL)	pUC19 (15 ng/μL)	2	2	2	2	2	2	2	2	2	2	2	2	2	2
AL- VIII (100 μM)	AL-VIII (2.5 μM)	~	~	1	1	1	1	1	~	~	1	1	1	1	1
Phos Buffer (100 mM)	Phos Buffer (10 mM)	4	4	4	4	4	4	4	4	4	4	4	4	4	4
NaCl (1 M)	NaCl (150 mM)	6	6	6	6	6	6	6	~	~	~	~	~	~	~
KCl (1 M)	KCl (260 mM)	10.4	10.4	10.4	10.4	10.4	10.4	10.4	~	~	~	~	~	~	~
	ddH_20	17.6	17.6	16.6	16.6	16.6	16.6	16.6	34	34	33	33	33	33	33
Light (min)		0	60	0	8	10	20	60	0	60	0	8	10	20	60

2.5 Preparation of Agarose Gel Electrophoresis

To prepare a 1.5% gel, 3.0 g agarose was dissolved in 200 mL 1X TAE buffer. The mixture was heated to molten in a microwave and 20 μL of ethidium bromide (0.5 μg/mL in H_2O) was added. The liquid gel was poured into a gel box and allowed to set. Once the gel solidified, the box was filled with 1X TAE running buffer and 20 μL of the previously prepared photocleavage samples were loaded onto the wells. More ethidium bromide was added to the running buffer and electrophoresis was conducted at 161 V for 3 h. Gel images were visualized on a VWR Scientific Transilluminator and captured using a Canon Powershot A4640.

2.6 UV-visible Studies with CT-DNA

2.6.1 Dye Titration without Salt

UV-visible experiments were conducted by preparing samples containing compound **1** or **2** was and a combination of the following stock solutions:

475 μL ddH_2O
50 μL 10 mM Sodium phospate buffer (pH 7)
25 μL 50 μM Dye

The solution was allowed to equilibrate in the dark for 60 min. Absorbance spectrum of the compound was recorded after 1 h. CT-DNA (0 – 485 μM) was added to the sample in 20 μL increments and allowed to equilibrate for in the dark for 60 min after each turn. A spectrum was recorded after each equilibration in a 1 cm quartz cuvettes (Starna). Absorbance data were plotted as a function of wavelength. Absorbance was corrected for volume changes using the equation below for all UV-visible experiments:

$$A_{corr} = A_{exp} \times (1000 + V)/1000$$

2.6.2 Dye Titration with Addition of Salt

Sample containing compound **1** or **2** was prepared by combining the following stock solutions:

220 μL ddH_2O
50 μL 10 mM Sodium phospate buffer
25 μL 50 μM Dye
75 μL 150 mM NaCl
130 μL 260 mM KCl

The solution was allowed to equilibrate in the dark for 60 min. Absorbance spectrum of the compound was recorded after an hour. CT-DNA (0 – 485 μM) was added to the sample in 20 μL increments and allowed to equilibrate for in the dark for 60 min after each addition. A spectrum was recorded after each equilibration in 1cm quartz cuvettes (Starna). Absorbance data was plotted as a function of wavelength.

2.7 DNA Melting Studies

Individual 1 mL solutions containing 30 uM bp of CT-DNA in 10 mM sodium phosphate buffer at pH 7.0 were prepared with varying concentrations (0-10 μM) of compound **1** or **2**. Samples were equilibrated in the dark for 60 min and transferred into 1.5 mL cuvettes (Starna). DNA absorbance was measured as a function of increasing temperature from 25 to 95 ^{o}C at a rate of 0.5 ^{o}C min^{-1}. Data was analyzed using KaleidaGraph version 3.6.4 software. Graphs were normalized using Equation 1 and the first derivative $\Delta A_{260}/\Delta T$ of the plot was using to determine the T_m of CT-DNA in the presence of each dye.

$$A_{Normalized} = \frac{|A_{CT\text{-}DNA} - A_{lowest}|}{|A_{highest} - A_{lowest}|} \qquad (1)$$

3 Results and Discussion

3.1 Synthesis of *N,N*-Dimethyl-*N'*-(9-methylanthracenyl)ethylenediamine

Compound **2** was synthesized according to procedures described by Bag and Bharadwaj [37]. Final product was obtained from the reaction of 9-anthraldehyde with *N,N*-dimethylethylenediamine. A brown semi-solid product **2** was obtained as expected in the literature. The product was characterized using ^{1}H NMR and ESI MS. The literature reported a yield of 92% and our experimental yield was 83%.

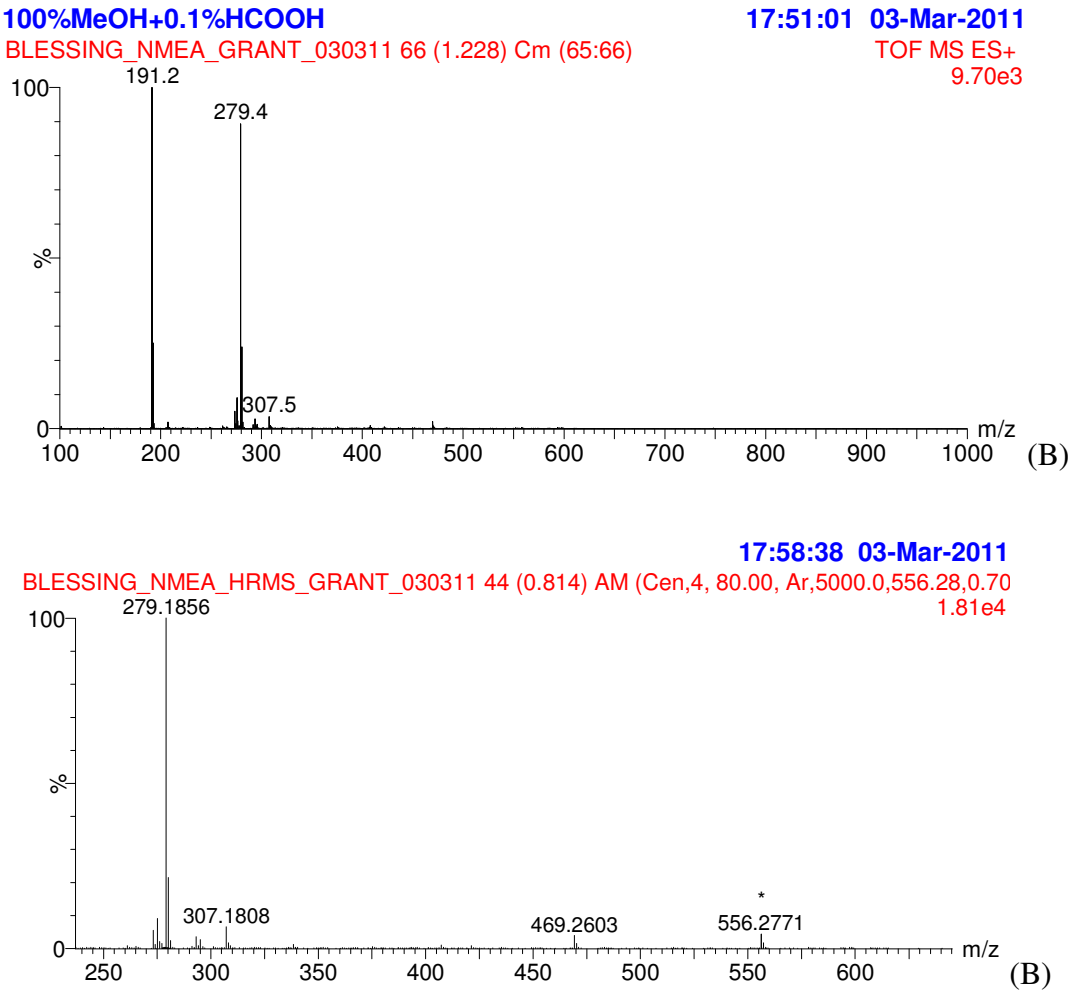

Figure 3.1: (A) ESI-MS, (B) HRMS of compound **2**.

The mass spectrum of the product showed a molecular ion peak M+H at 279.4 m/z. This provided strong evidence of that the product was indeed synthesized since its average mass is 278.4 g/mol and the addition of a proton will give the observed parent peak. Furthermore, the mass spectrometry analysis reported an exact mass of 279.1856 and the calculated mass of the compound is 279.1861. A strong fragment peak is also observed at 191.2 indicating the dissociation of the product to give the anthracene (An-CH_2^-) fragment. This would be the most stable ion since the secondary nitrogen would form a stable cation if protonated and dissociate form the compound.

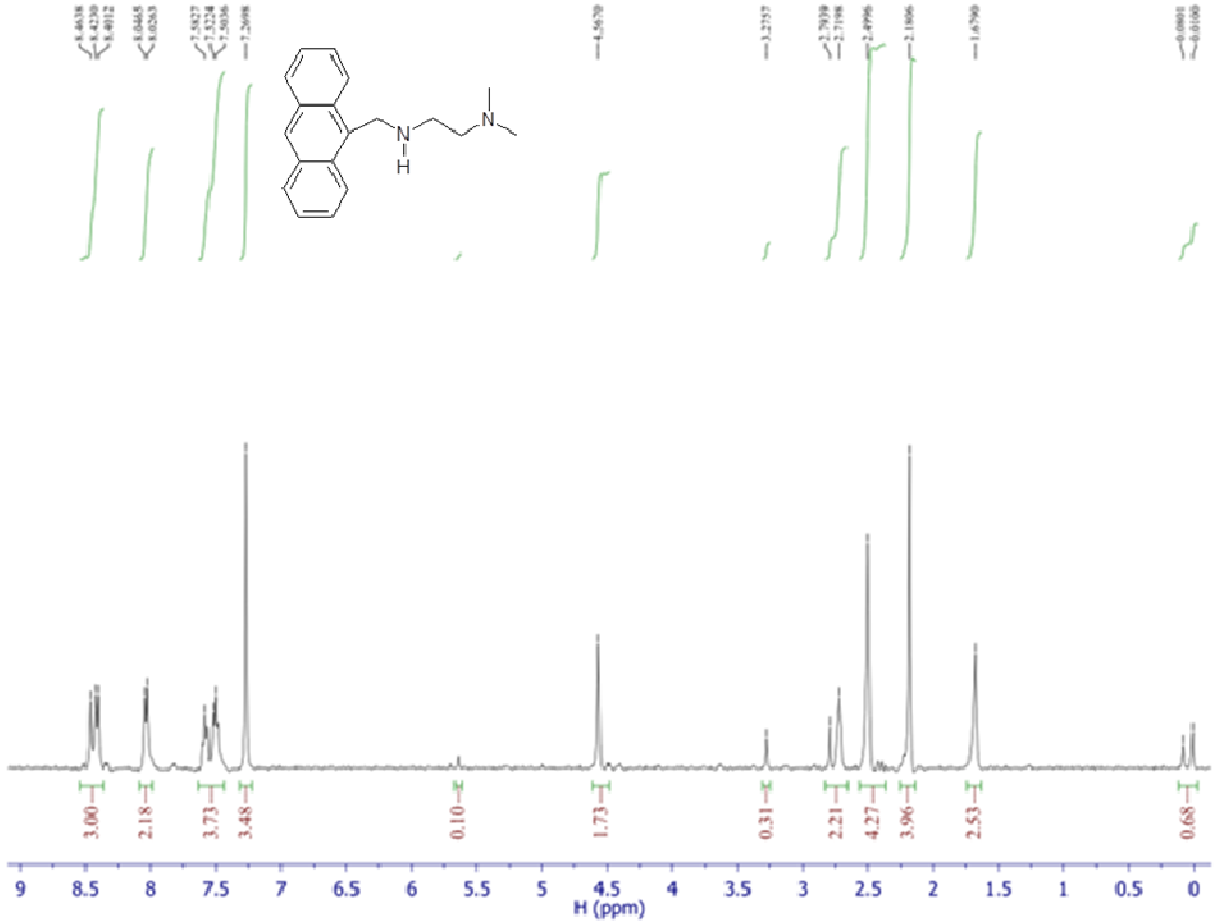

Figure 3.2: ^{1}H NMR of compound **2** (400 MHz, $CDCl_3$, 25°C): δ = 2.17 (s, 6H, 2×CH_3), 2.49 (s, 2H, CH_2), 2.72 (t, 2H, CH_2), 4.73 (s, 2H, An-CH_2), 7.44 (t, 2H, An-H), 7.52 (t, 2H, An H), 7.88 (d, 2H, An-H), 8.42 (m, 3H, An-H).

The ^{1}H NMR spectrum showed supporting evidence of compound **2** synthesis. Chemical shifts were similar to what was reported in the literature [37]. The proton attached to the secondary amine and the methyl group directly attached to the anthracene ring were not observed on the spectrum. This could be due to induction and the charge density from the anthracene ring. It could also be due to experimental factors such as the solvent or temperature.

3.2 Photocleavage Experiments

DNA photocleavage of pUC19 plasmid was evaluated as a function of decreasing concentration (10 - 0 μM) of bis-anthracene **1**, and its mono-anthracene analog **2** in the presence and absence of salt. These reactions were conducted mimicking physiological conditions by adding 150 mM NaCl and/or 260 mM KCl to the reaction. The aim of these experiments was to observe the effects of salt addition of photocleavage yields with both compounds. The samples were aerobically irradiated for 60 min in Rayonet Photochemical Reactor. Figures 3.3 - 3.10 show that upon irradiation by 350 nm light, supercoiled pUC19 plasmid DNA is converted to its nicked and linear forms with increasing concentration of compounds **1** or **2**. The addition of 260 mM KCl and 150 mM NaCl either enhanced or inhibited DNA photocleavage, as explained on the following pages.

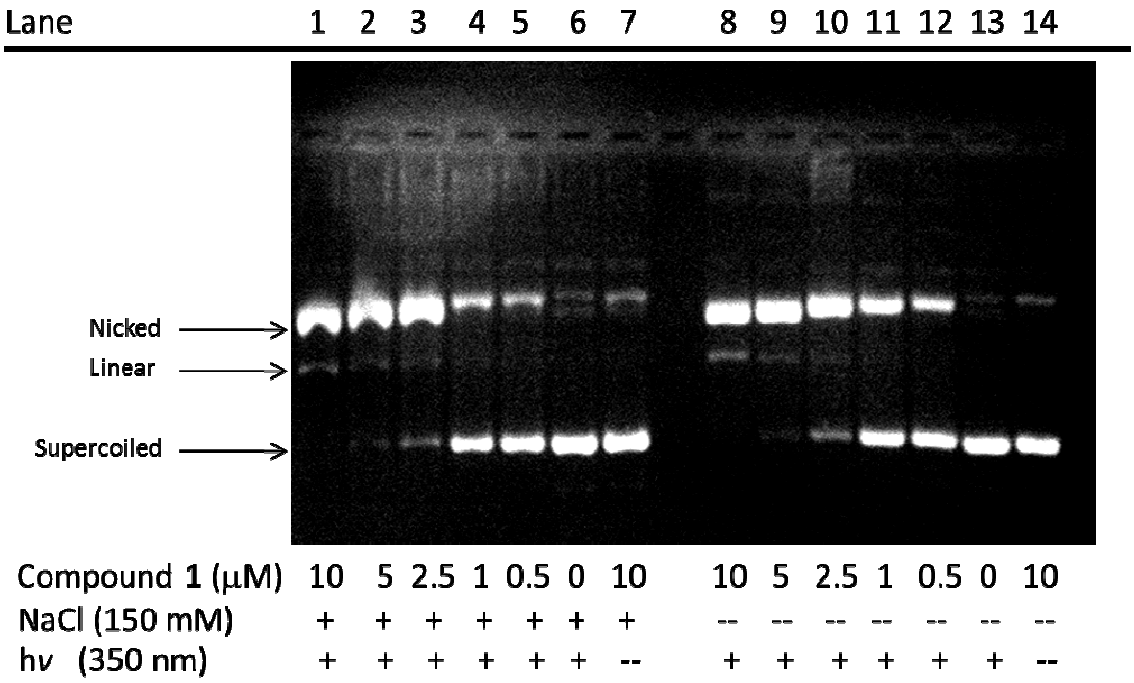

Figure 3.3: Image of 1.5% non-denaturing agarose gel depicting photocleavage of 23 μM bp of pUC19 with decreasing concentration of **1** (10 - 0 μM). Reactions contained 10 mM sodium phosphate buffer (pH 7.0) with lanes 1 - 7 containing 150 mM NaCl (350 nm, 60 min).

In Figure 3.3, the addition of NaCl had no effect in enhancing photocleavage of the DNA. At concentrations of 10 – 2.5 μM compound **1** showed no enhancement of DNA photocleavage but a slight inhibition cleavage at low concentrations (1 – 0.5 μM) with the addition of 150 mM NaCl.

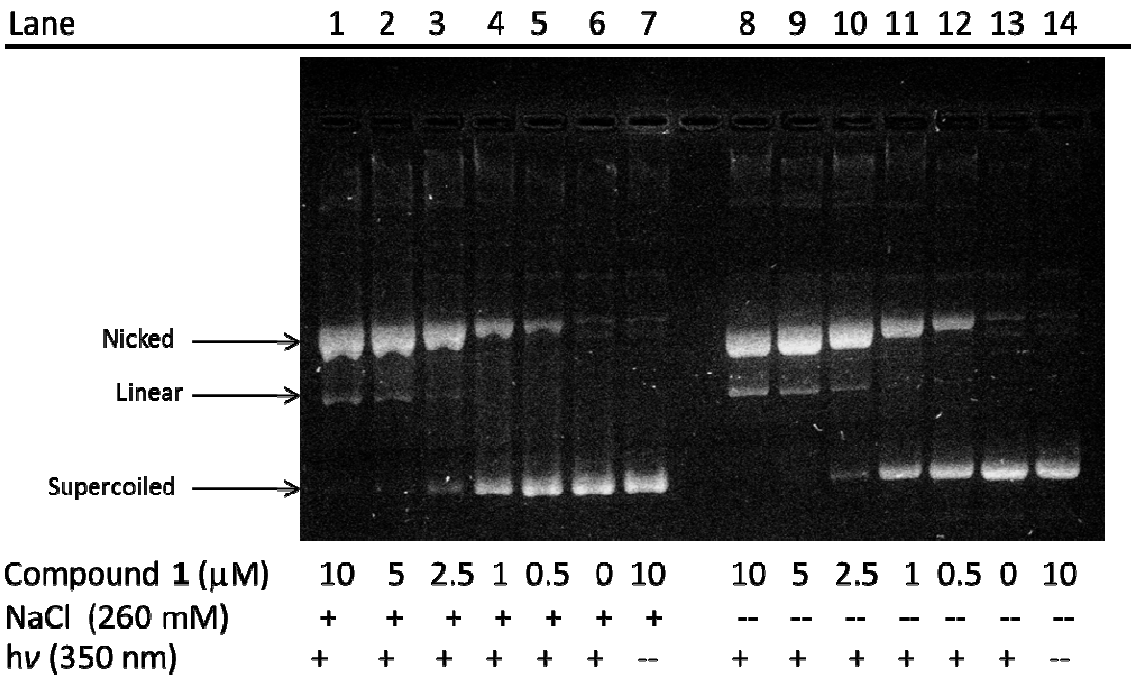

Figure 3.4: Image of 1.5 % non-denaturing agarose gel depicting photocleavage of 23 μM bp of pUC19 with decreasing concentration of **1** (10 - 0 μM). Reactions contained 10 mM sodium phosphate buffer (pH 7.0) with lanes 1-7 containing 260 mM NaCl (350 nm, 60 min).

Next a photocleavage experiment was conducted to evaluate the effect of increasing the concentration of sodium chloride on photocleavage yields. As observed in the Figure 3.4, there was no difference in photocleavage enhancement with the addition of a higher concentration of NaCl. Plasmid cleavage was still inhibited at concentrations of compound **1** (≤ 1 μM).

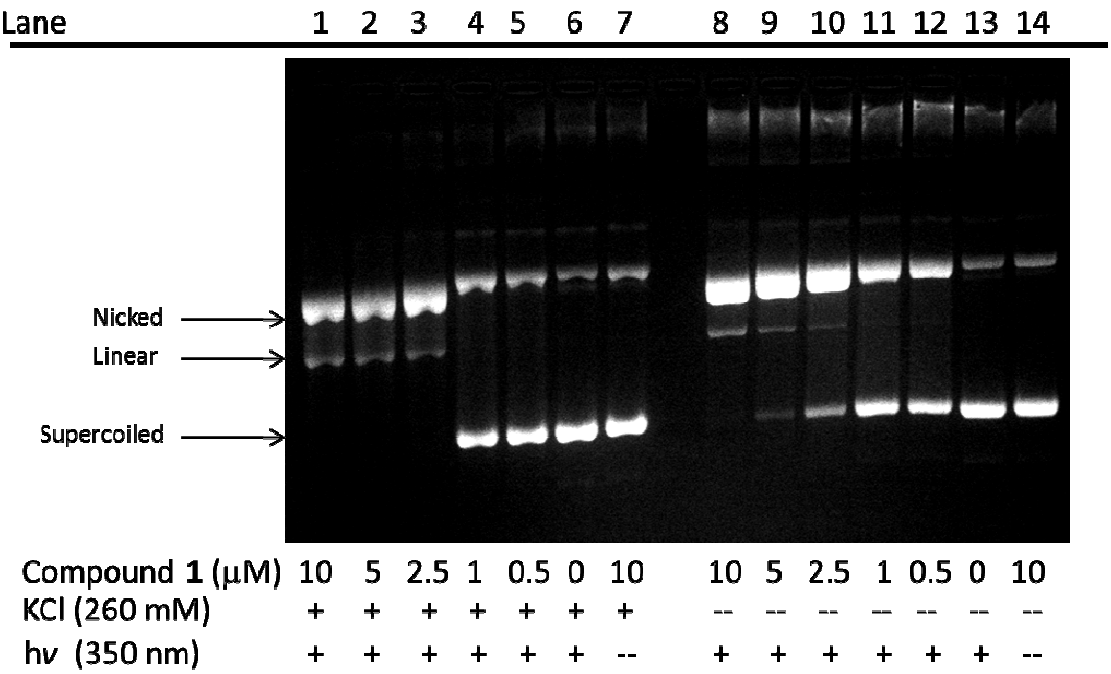

Figure 3.5: Image of 1.5% non-denaturing agarose gel depicting photocleavage of 23 μM bp of pUC19 with decreasing concentration of **1** (10 - 0 μM). Reactions contained 10 mM sodium phosphate buffer (pH 7.0) with lanes 1 - 7 containing 260 mM KCl (350 nm, 60 min)

DNA photocleavage was then evaluated in the presence of 260 mM KCl. Figure 3.5 shows an increase in photocleavage at 5 and 2.5 μM with the addition of 260 mM KCl. The supercoiled bands observed in lanes 9 and 10 are not present in lanes 2 and 3. Photocleavage inhibition was also observed at concentrations of compound ≤ 1 μM. There is slightly more nicked DNA in lanes 11 and 12 than lanes 5 and 6. When compared to the addition of 150 mM NaCl (Figure 3.3), lanes 2 and 3 show an increase of nicked DNA.

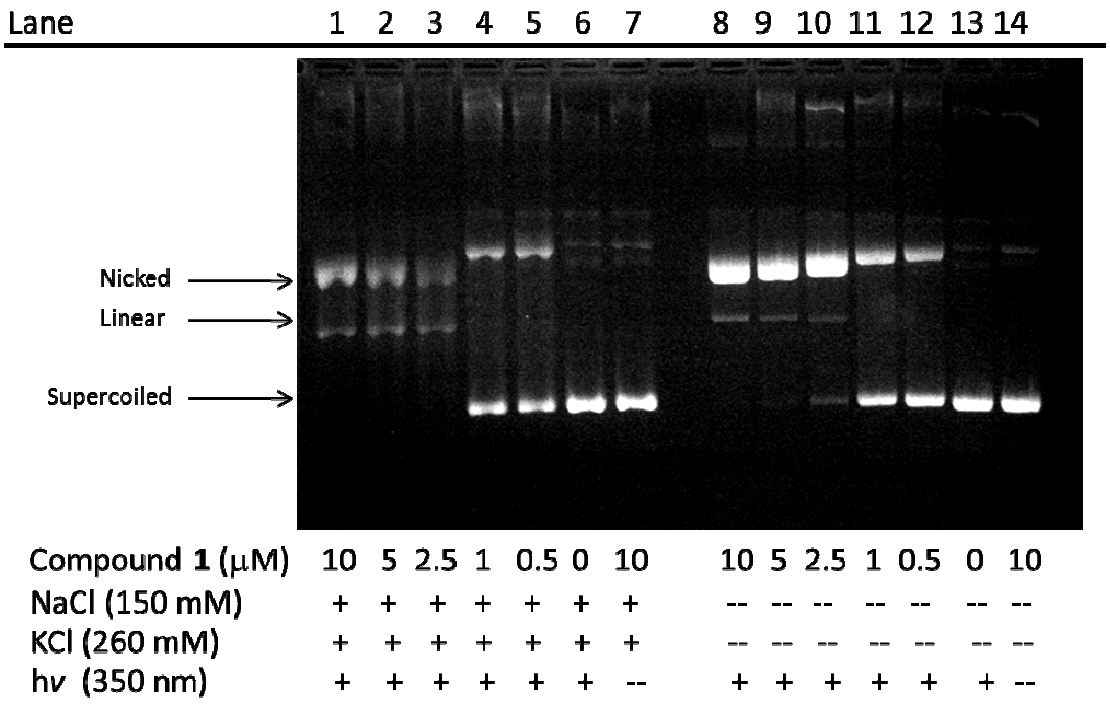

Figure 3.6: Image of 1.5% non-denaturing agarose gel depicting photocleavage of 23 μM bp of pUC19 with decreasing concentration of **1** (10 - 0 μM). Reactions contained 10 mM sodium phosphate buffer (pH 7.0) with lanes 1 - 7 containing 260 mM KCl and 150 mM NaCl (350 nm, 60 min).

The next step was to conduct a titration experiment in the presence of both 150 mM NaCl and 260 mM KCl. Figure 3.6 also shows an enhancement in cleavage with the addition of both salts when compared to the addition of 150 mM NaCl. The picture shows the most enhancement in cleavage at higher concentrations of compound (5 – 2.5 μM). There is an increase of linear DNA at 5 μM (lane 2) with the addition of both salts. The supercoiled DNA present in lane 10 is no longer present in lane 3 with the addition of salt. There is inhibition of photocleavage at concentration of compound ≤ 1 μM. This effect is similar to the amount of cleavage observed for the addition of 260 mM KCl.

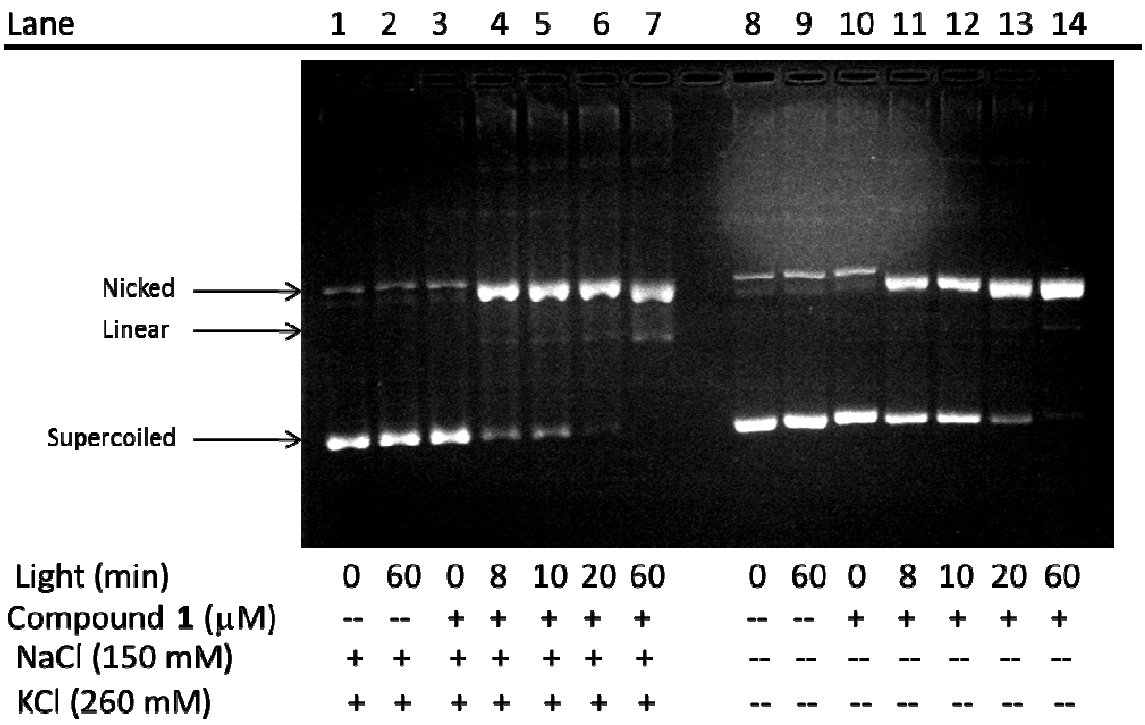

Figure 3.7: Image of 1.5 % non-denaturing agarose gel depicting photocleavage of 23 μM bp of pUC19 with 2.5 μM of **1**. Reactions contained 10 mM sodium phosphate buffer (pH 7.0) with lanes 1 - 7 containing 150 mM NaCl and 260 mM KCl irradiated at 350 nm for 0-60 min.

In order to evaluate the kinetics of photocleavage of pUC19 with compound **1** as a function of time, a time course experiment was conducted. In this experiment, 2.5 μM of **AL-VIII 23** was used because the transition from supercoiled to nicked DNA was more distinct in the salt titration experiments. With addition of 150 mM NaCl and 260 mM KCl, pUC19 plasmid DNA is almost completely cleaved when irradiated for 20 min at 350 nm. The picture also shows photocleavage enhancement with the addition of salt at all time points of irradiation.

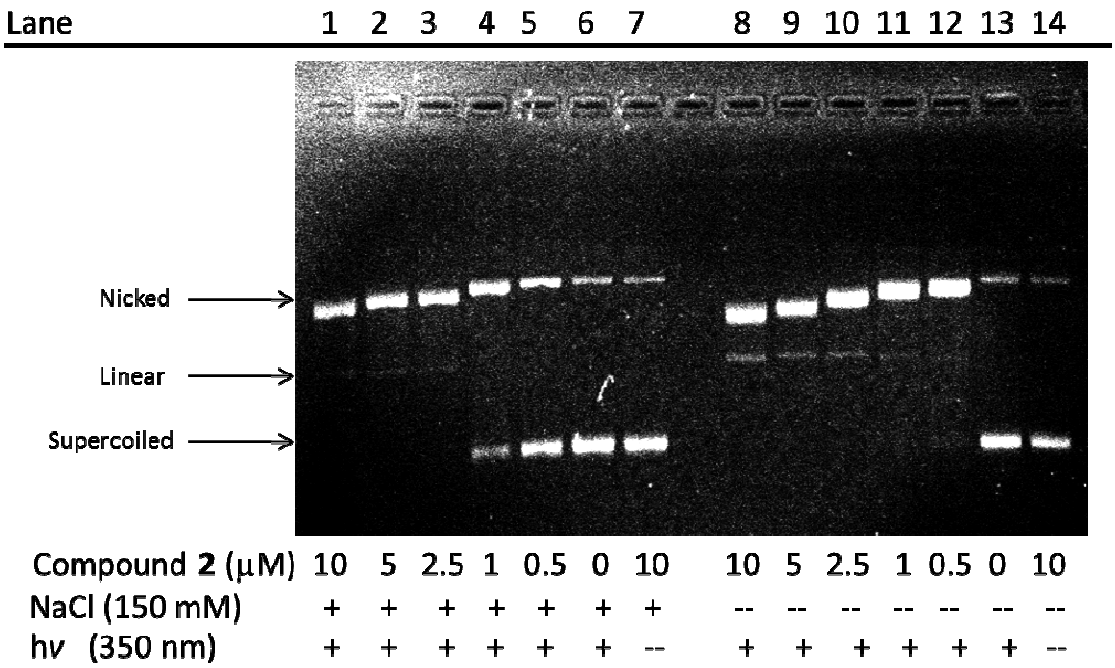

Figure 3.8: Image of 1.5% non-denaturing agarose gel depicting photocleavage of 23 μM bp of pUC19 with decreasing concentration of **2** (10 - 0 μM). Reactions contained 10 mM sodium phosphate buffer (pH 7.0) with lanes 1 - 7 containing 150 mM NaCl (350 nm, 60 min).

With the synthesis of the **2**, the mono-anthracene analog of compound **1**, photocleavage experiments were conducted to monitor cleavage yields in the presence of salt. In Figure 3.8, the addition of 150 mM NaCl showed marked inhibition of photocleavage at 1.0 and 0.5 μM concentrations of **2**. This image also shows evidence of a decrease in linear DNA from 10 – 2.5 μM concentrations of compound with the addition of NaCl.

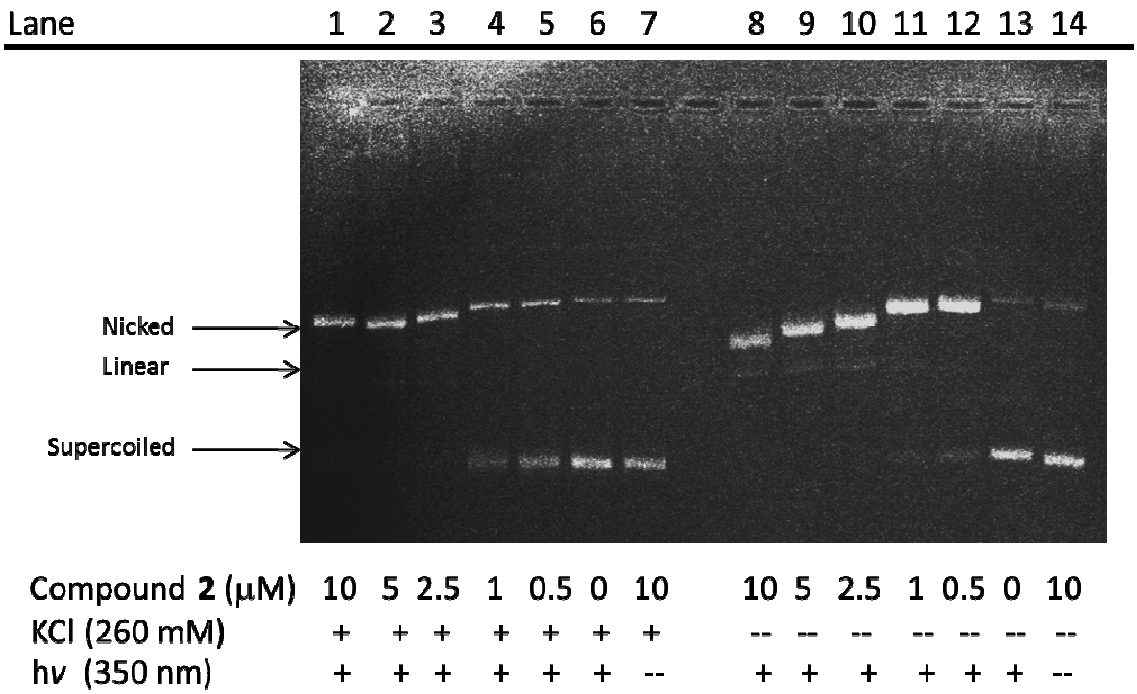

Figure 3.9: Image of 1.5 % non-denaturing agarose gel depicting photocleavage of 23 μM bp of pUC19 with decreasing concentration of **2** (10 - 0 μM). Reactions contained 10 mM sodium phosphate buffer (pH 7) with lanes 1 - 7 containing 260 mM KCl (350 nm, 60 min).

Next, a titration experiment of compound **2** with the addition of 260 mM KCl was conducted. Figure 3.9 indicates that the addition of 260 mM KCl reduced photocleavage yields. This result is very similar to the 150 mM NaCl addition experiment, showing inhibition of DNA cleavage at low dye concentration (1 - 0.5 μM).

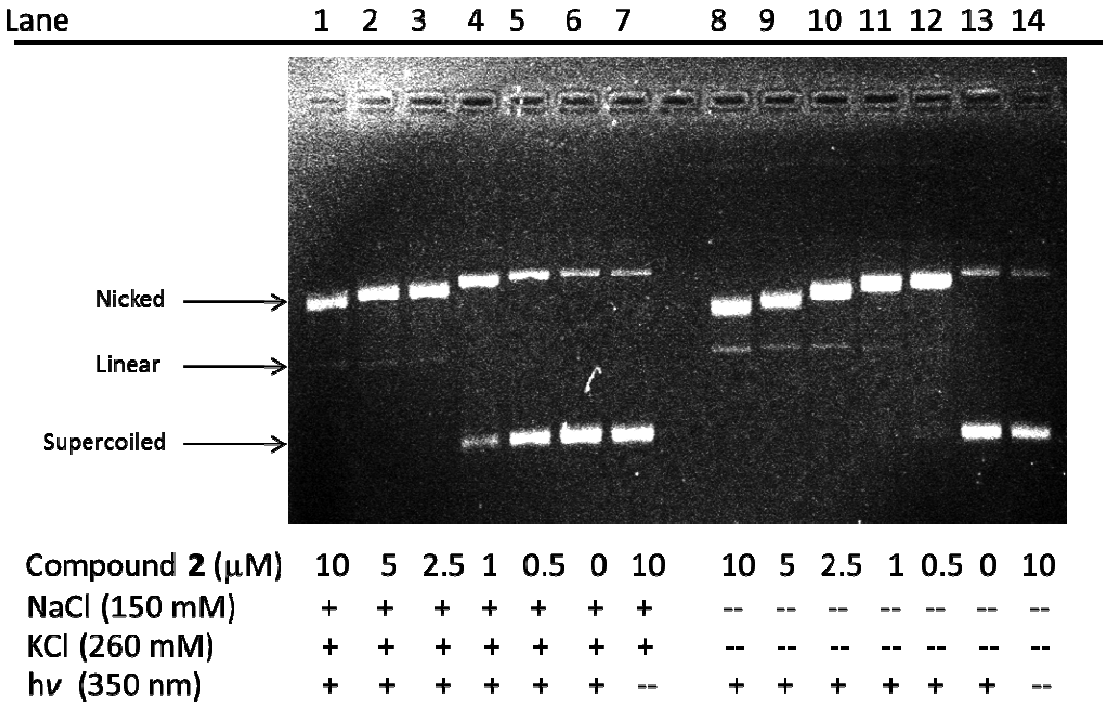

Figure 3.10: Image of 1.5% non-denaturing agarose gel depicting photocleavage of 23 uM bp of pUC19 with decreasing concentration of **2** (10 - 0 μM). Reactions contained 10 mM sodium phosphate buffer (pH 7) with lanes 1 - 7 containing 260 mM KCl and 150 mM NaCl (350 nm, 60 min).

Lastly, a photocleavage experiment with the addition of both 150 mM NaCl and 260 mM KCl was conducted. In contrast to the addition of 260 mM KCl, the addition of both salts did not appear to change photocleavage at concentrations of **2** ranging from 10 – 2.5 μM. However, significant inhibition were still observed at low concentrations of compound **2** (1 – 0.5 μM).

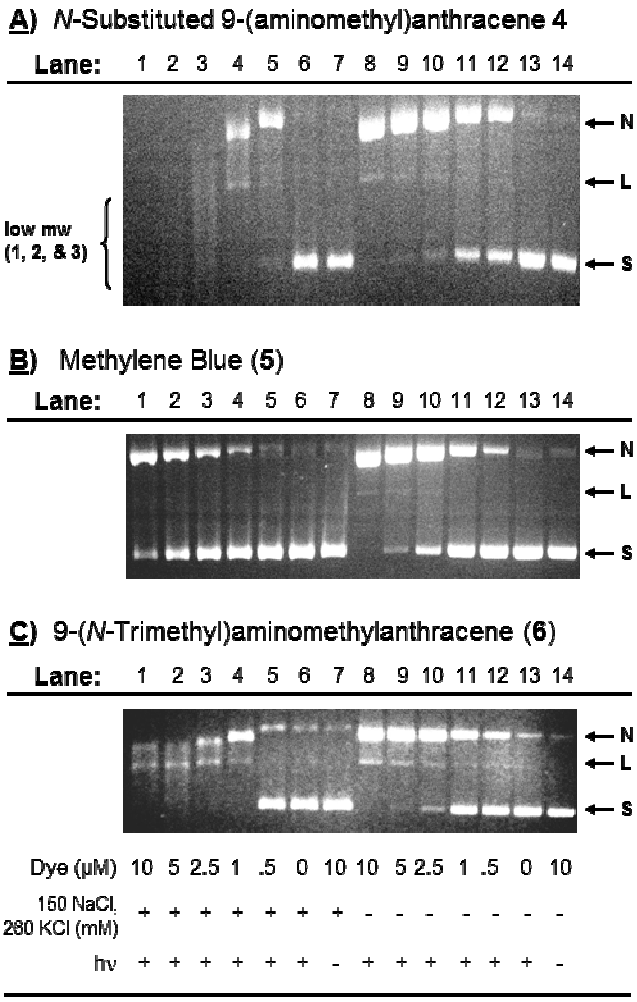

Figure 3.11: Agarose gel image of image of anthracene based chromophores with decreasing dye concentrations (10 - 0 μM) and addition of 150 mM NaCl, 260 mM KCl (lanes 1 - 7). Reactions contained 10 mM phosphate buffer (pH 7) and were irradiated at 350 nm for 60 min.

The gel images displayed in Figure 3.11 are experiments conducted in the Grant research group with experimental conditions similar to photocleavage of compound **1** and **2**. The compounds in Figure 3.12 were used to analyze the effects of salt concentration on DNA photocleavage. Compounds 4 and 6 (Figure 3.11) show more photocleavage enhancement than compound **1** and **2** with the addition of 150 mM NaCl and 260 mM KCl. UV-visible studies of compounds **4** and **6** showed indicated intercalation to the DNA helix and change in conformation to external binding with the addition of both salts. Methylene blue **5** is a known DNA

intercalator and was used as a control during these experiments. As seen in the picture above, the photocleavage yields for methylene blue show inhibition of photocleavage with the addition of salt. This result suggests that external agents are more effective at cleaving DNA than intercalating agents, with the addition of salt. These results also suggest that compound **2** could possibly be an intercalator since inhibition of photocleavage is observed with the addition of salt.

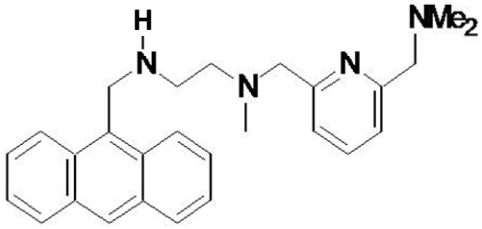

ML-Vic (**4**)

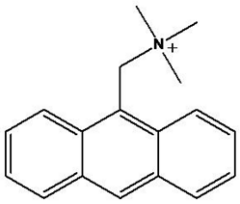

9-MATM (**6**)

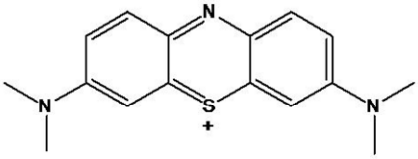

Methylene Blue (**5**)

Figure 3.12: Structure of photocleavage dyes.

3.3 UV-visible Titrations

UV-visible titrations were used to monitor the DNA binding of compounds **1** and **2**. The reactions were recorded in the presence of increasing concentrations of CT-DNA (0 – 485 μM bp). The titration samples were allowed to equilibrate in the dark for 60 min after each DNA addition. The solutions in Figures 3.13 and 3.15 also contained 150 mM NaCl and 260 mM KCl, mimicking physiological conditions in the cell nucleus [27]. Absorbance was corrected for volume changes.

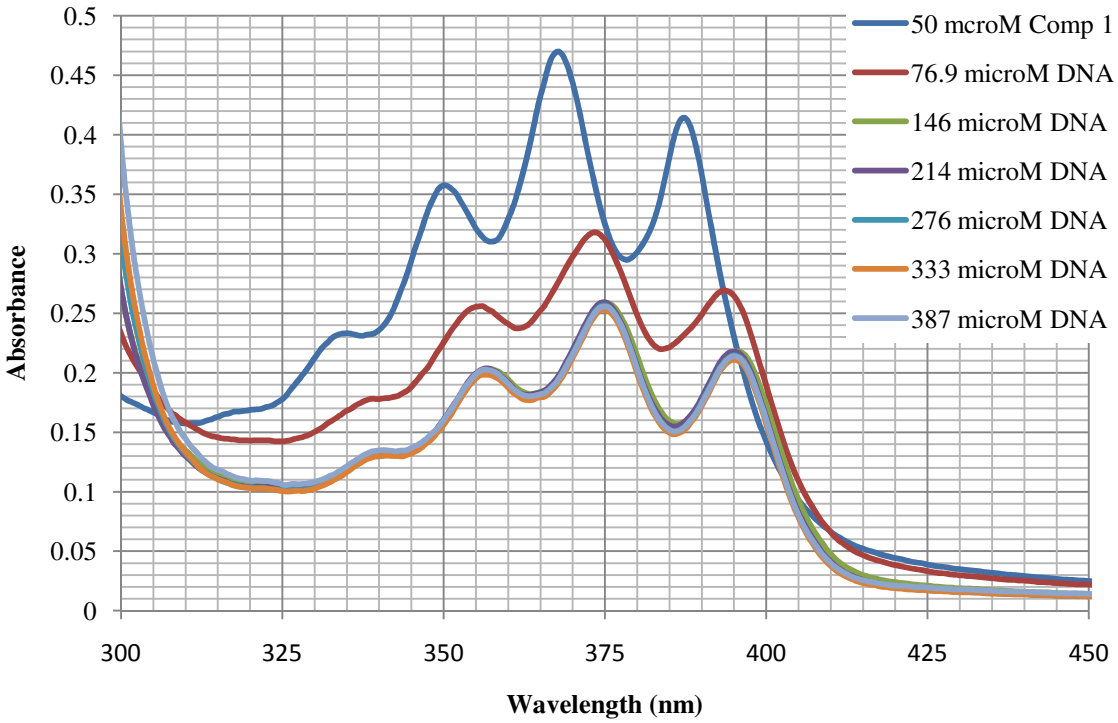

Figure 3.13: UV-visible spectra of 50 μM of **1** with increasing concentrations of CT-DNA. The solution contained 10 mM phosphate buffer (pH 7.0). Spectra were adjusted for dilution of sample.

UV-visible studies of compound **1** with increasing concentrations of CT-DNA (0 – 387 μM) were performed to monitor absorbance and maximum wavelenghts as the compound binds

to DNA. Figure 3.13 compares the absorbance curve of **1** with and without the addition of CT-DNA. This figure shows a hypochromic and bathochromic shift with increasing concentrations of DNA. This shift in absorbance and wavelength is evidence of DNA intercalation [20, 38-40]. The plot above also indicates that compound **1** readily intercalates between base pairs, reaching saturation by 145 μM bp CT-DNA.

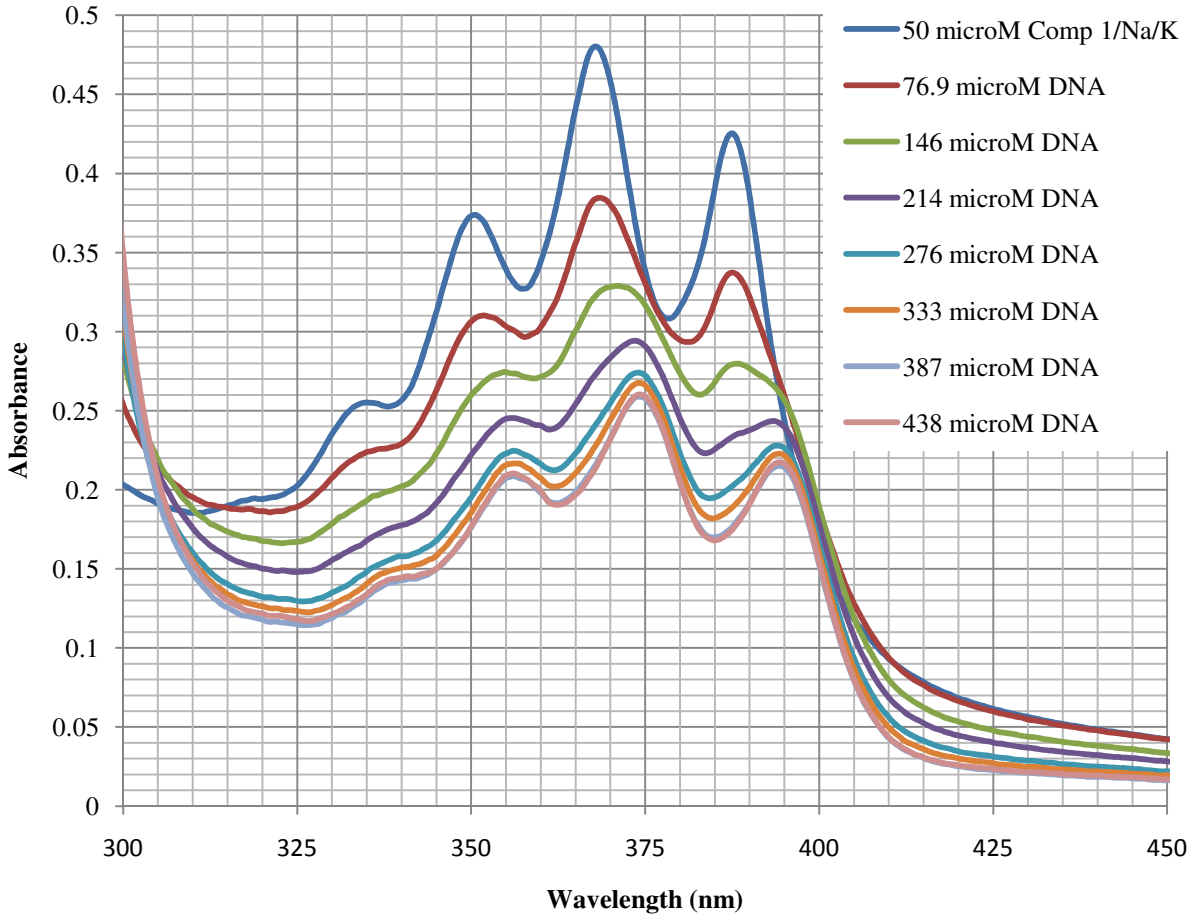

Figure 3.14: UV-Visible spectra 50 µM of **1** with increasing concentration of CT-DNA and addition of 260 mM KCl, 150 mM NaCl in 10 mM phosphate buffer (pH 7.0). Spectra were adjusted for dilution of sample.

Figure 3.14 compares the absorbance curve of **1** in 150 mM NaCl and 260 mM KCl with the compound in the presence of increasing concentrations of CT- DNA. This figure shows hypochromicity and bathochromicity increasing concentration of DNA. As DNA concentration is increased, the spectral changes observed in Figure 3.13 (no added salt) become more apparent. The spectral changes occurs gradually as more DNA is added to the sample. The spectrum also shows that binding of compound **1** reaches saturation at 387 µM bp of DNA.

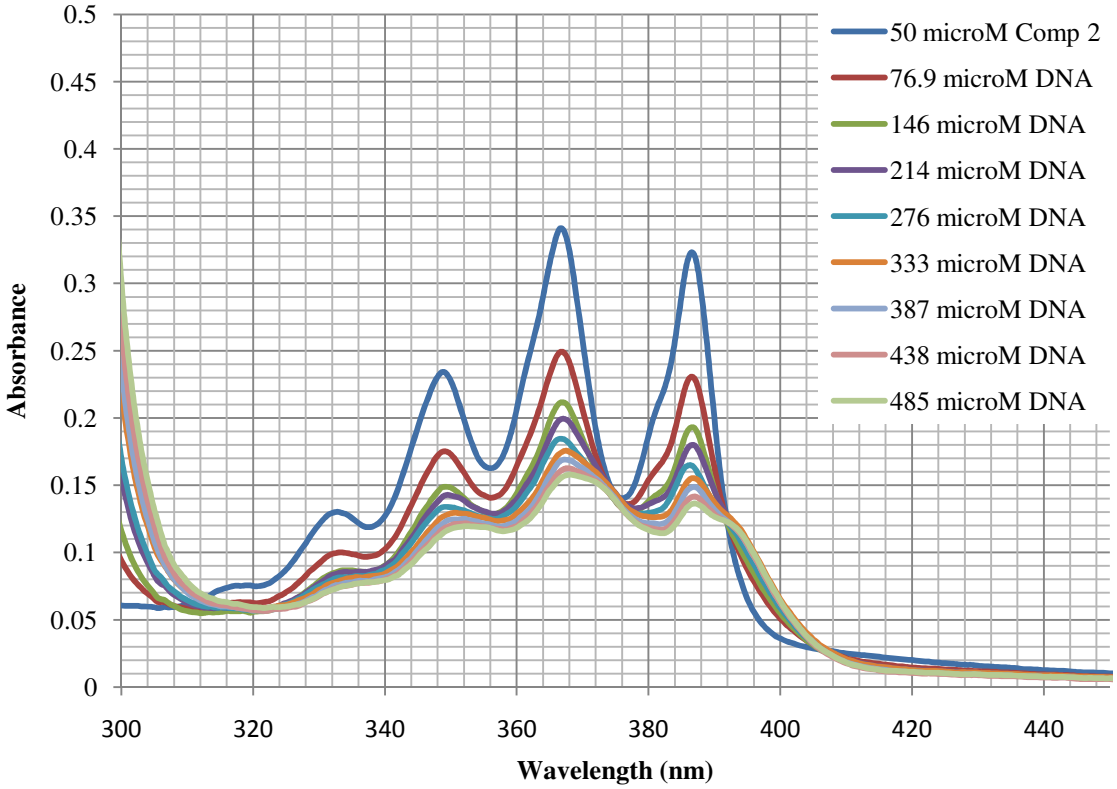

(A)

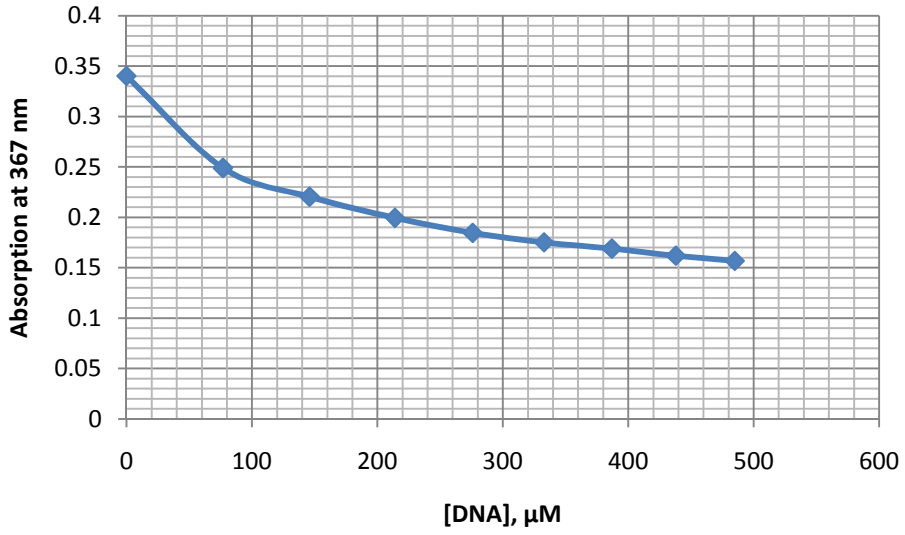

(B)

Figure 3.15: (A) UV-visible spectra of 50 µM of **2** with increasing concentrations of CT DNA in 10 mM phosphate buffer (pH 7.0). (B) Plot of absorption of **2** at 367 nm as a function of CT DNA concentration. Spectra were adjusted for dilution of sample.

Similarly, the absorbance spectra of compound **2** was also monitored, seeing as it showed no enhance of photocleavage with addition of salt. Figure 3.15 compares the absorbance curve of **2** with and without the addition of CT DNA. This figure shows a hypochromic shift with increasing concentrations of DNA. There seems to be a shift from groove binding to intercalation mode as a shoulder starts to appear at 393 nm with an increase in DNA concentration. This spectrum also suggests that there are two binding modes present with a rapid decrease in absorbance initially and then more slowly as DNA concentration increases (Figure 3.15B). An isosbestic point is also observed at 392 nm (Figure 3.15A); this indicates the conversion of one type of chromophore to another. By the addition of 485 μM of DNA, a saturation point has still not been observed. Hence, compound **2** appears to bind to DNA with weaker affinity than compound **1**. Previous research conducted by Kumar and co-workers has shown that anthracene ligands that show a bathochromic and hypochromic shift in UV-visible spectra are DNA intercalators, while compound which show hypochromicity and no bathochromicity are DNA groove binders [20, 26].

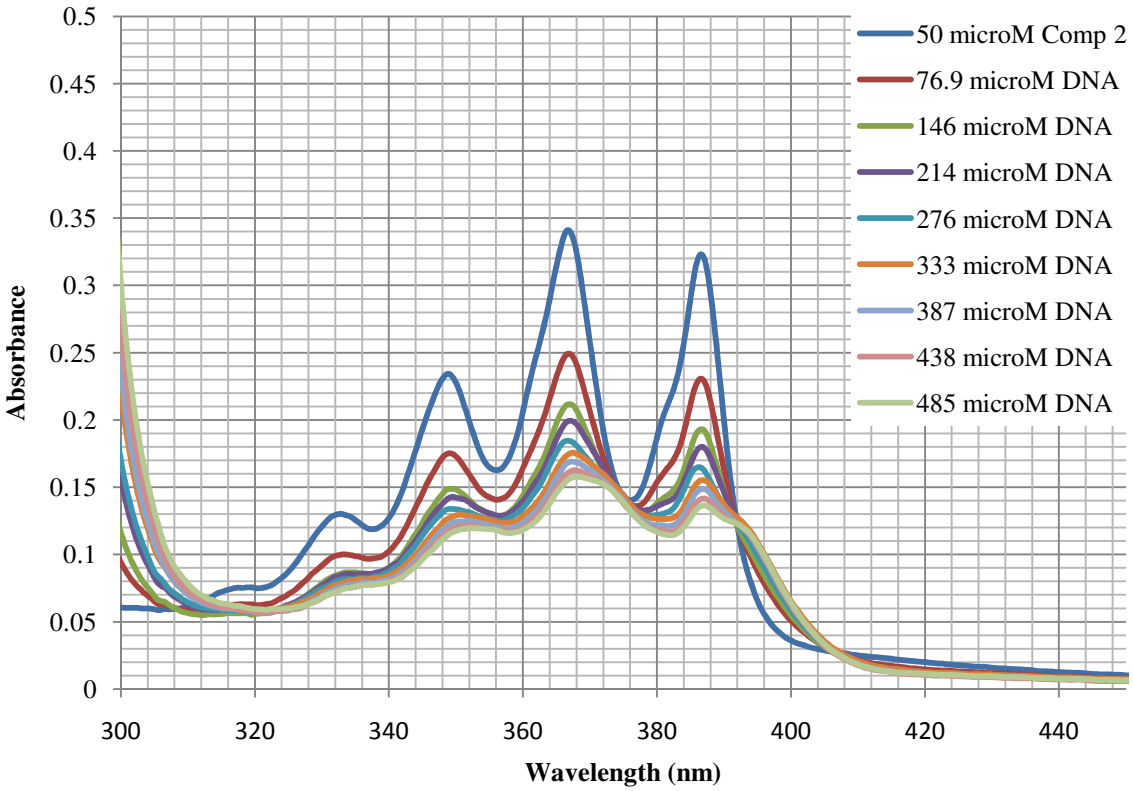

(A)

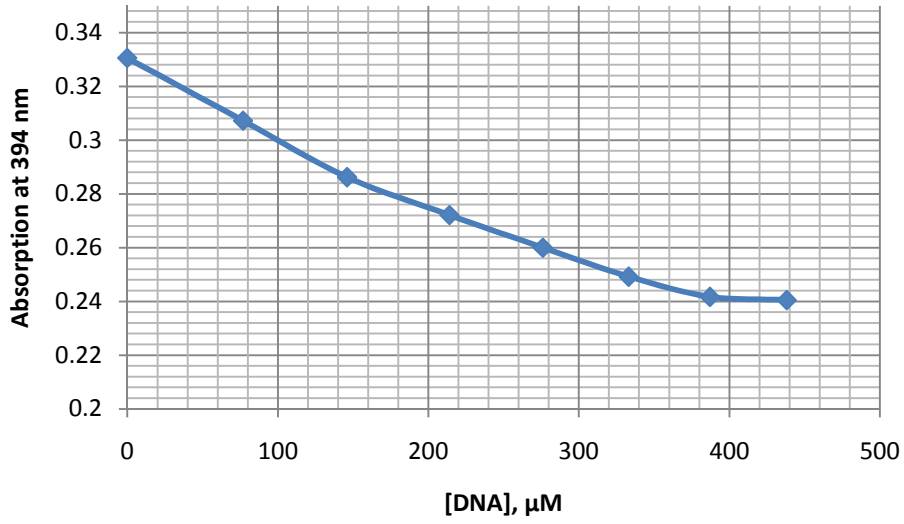

(B)

Figure 3.16: (A) UV-Visible spectra 50 µM of **2** in the presence of CT DNA, 260 mM KCl, and 150 mM NaCl in 10 mM phosphate buffer (pH 7.0). (B) Absorption of **2** at 367 nm as a function of CT-DNA concentration. Spectra were adjusted for dilution of sample.

Figure 3.16 compares the absorbance curve of **2** in 150 mM NaCl and 260 mM KCl with increasing concentrations of CT DNA. This figure shows hypochromicity but no bathochromicity with increasing concentration of DNA. When compared to the absorbance spectra without salt (Figure 3.15), the second λ_{max} is not present. The data are consistent with a model in which the compound is groove bound to the helix. Unlike the no salt experiment, compound **2** reached saturation at 387 μM bp of DNA with the addition of both salts. The shallow decrease in absorbance observed in the graph (Figure 3.16B) is characteristic of a groove binding agent [32].

Table 3.1: UV-visible maximum absorbance and wavelengths

Dye	**Abs (no salt)**	**λ_{max} (no salt)**	**Abs (salt)**	**λ_{max} (salt)**
50 μM Comp **1**	0.4699	367.5 nm	0.4802	368.0 nm
Comp **1** @ sat.	0.3407	375.0 nm	0.2130	374.0 nm
50 μM Comp **2**	0.3407	366.5 nm	0.3305	367.0 nm
Comp **2** @ sat	0.1578	368.0 nm	0.2417	367.0 nm

Table 3.1 compares the maximum absorbance and wavelengths of compound **1** and **2** with and without the presence of salt based on data from the UV-visible spectrum. At 50 μM concentration of both compounds, the addition of salt had barely any effect in increasing or decreasing the absorbance of the compound. On the other hand, the addition of salt had a significant effect on the wavelength at maximum absorbance shifting by 7.5 nm for compound **1** and 1.5 nm for compound **2**.

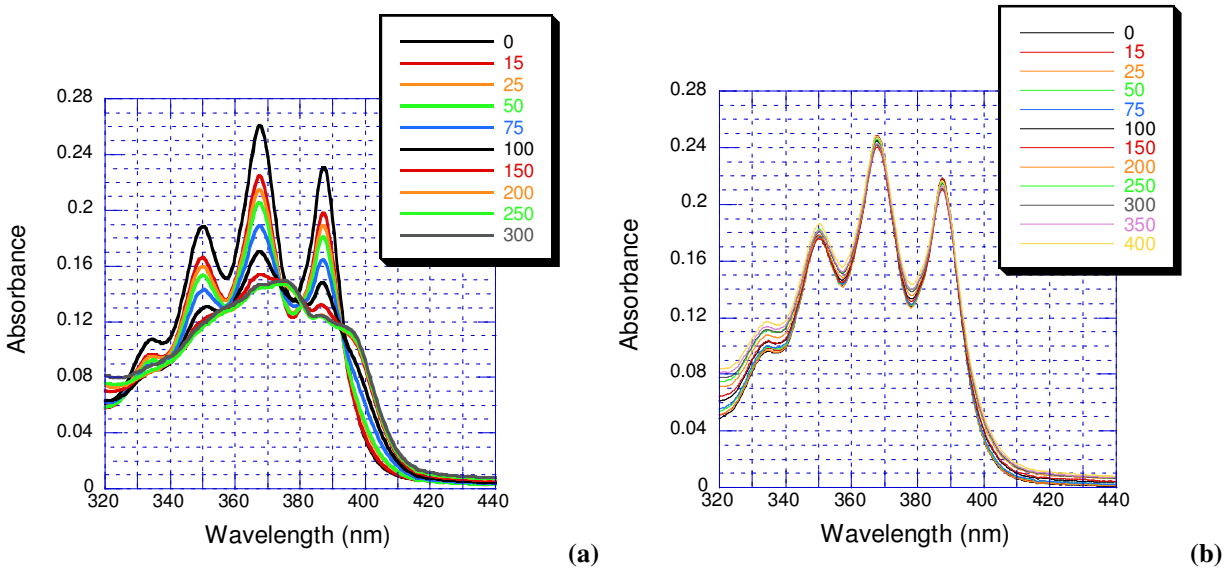

Figure 3.17: Displays UV-visible spectrum of an anthracene based chromophore **4** with increasing concentrations of CT DNA (a) and addition of 150 mM NaCl and 260 mM KCl (b) [31].

The image above was from an experiment conducted the Grant research group comparing the absorbance of an anthracene chromophore N^1-(anthracen-9-ylmethyl)-N^2-((6-((dimethylamino)methyl)pyridine-2-yl)methyl-N^1,N^2-dimentylethane-1,2-diamine (**4**). Under conditions of high salt concentration ~ 150 mM NaCl and 260 mM KCl, the compound shifts from intercalation to external mode. This change is conformation is characterized by a constant λ_{max} and very minimal change in absorbance as the DNA concentration increases.

3.4 DNA Melting Studies

DNA thermal denaturation studies were used to assess the binding affinity and stabilization of the duplex by compound **1** or **2**. Most DNA intercalators are known to stabilize the helix by increasing π-π stacking and electrostatic interactions. This increasing in stability also leads to an increase in DNA melting temperature (T_m) [12]. The T_m is the point at which half the DNA is double stranded and the other half is single stranded. In experiments testing for T_m values, 30 μM bp CT DNA were used to evaluate its stability with increasing concentrations of either **1** or **2**. Reaction samples containing deionized water, 10 mM sodium phosphate buffer, CT DNA, and anthracene dye were allow to equilibrate in the dark for 60 min before undergoing thermal denaturation.

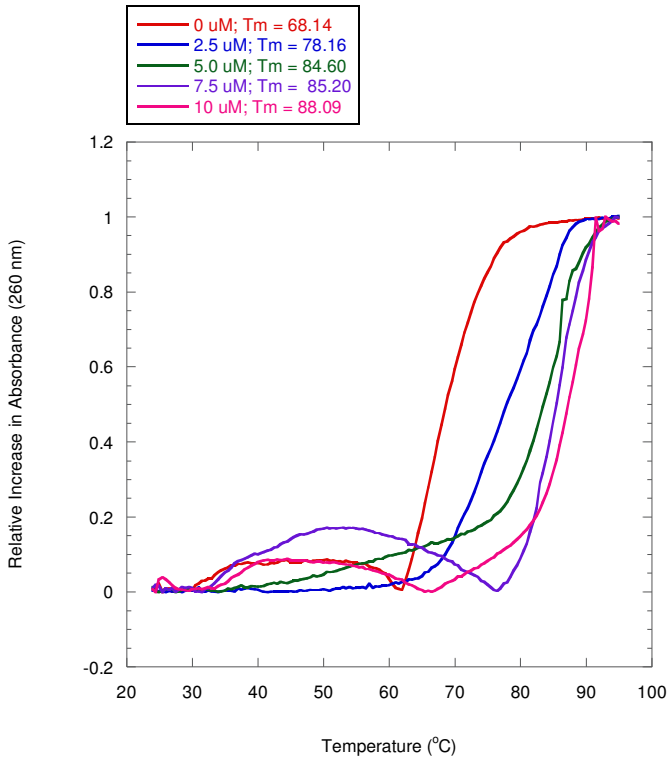

Figure 3.18: Thermal melting curves of 30 μM bp CT DNA with addition of **1** (0 – 10 μM) in 10 mM sodium phosphate buffer (pH 7.0).

The figure above shows that the melting temperature of calf thymus DNA increases with increasing concentrations of compound **1**. At 10 μM of **1**, an average ΔT_m of 21 ^oC is observed. Such a high increase in T_m is characteristic of a strong ligand/DNA interaction often observed in bis-intercalators [12].

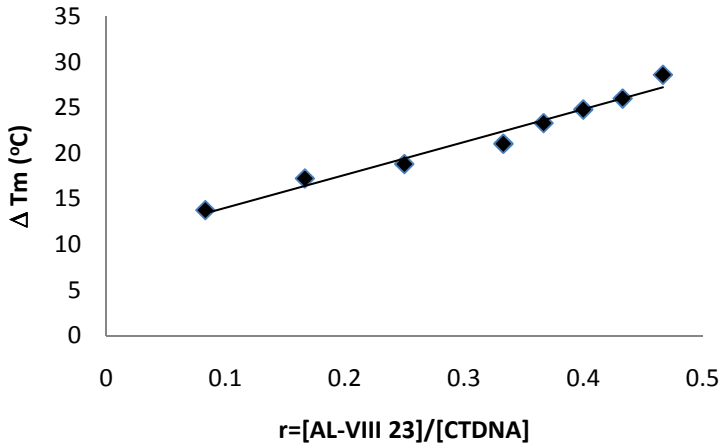

Figure 3.19: Plot of the ΔT_m as a function of the ratio of the concentration of **1** to the concentration of CT DNA.

The figure above shows a linear relationship between the change in melting temperature and the **r** value (the ratio of the dye concentration to DNA concentration). The melting temperature at saturation was not obtained because the instrument could only go up to 95^oC.

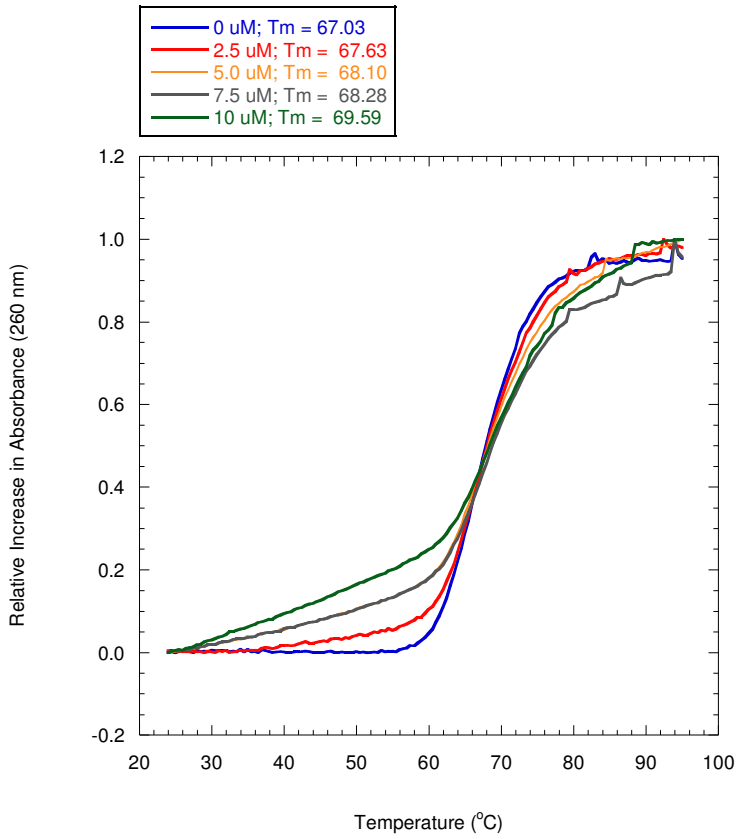

Figure 3.20: Thermal melting curves of 30 µM bp CT DNA with addition of **2** (0 – 10 µM) in 10 mM sodium phosphate buffer (pH 7.0).

The figure above shows that the melting temperature of calf thymus DNA increases with increasing concentrations of compound **2**. At 10 µM of **1**, a ΔT_m of 2 °C is observed. Unlike the bis-anthracene, very little increase in melting temperature is observed when **2** is added. These data agree with the UV-visible titrations suggesting that **2** weakly associates with the DNA helix. Groove binding anthracenes usually have very small ΔT_m values [38]. Hence, this result complies with the UV-visible data

4 Conclusion

Upon completion and analysis of photocleavage experiments, one can conclude that compound **1** and **2** are capable of inducing cleavage of DNA when activated by 350 nm light. It can also be concluded that DNA cleavage is enhanced at high concentrations of the compound **1** (10-2.5 μM) and inhibited at low concentrations (1.0-0 μM) with addition of salt. The addition of KCl enhances photocleavage whereas lower yields are observed with the addition of NaCl. The addition of both salts showed more cleavage than the addition of the single potassium chloride salt. Importantly, the high levels of cleavage caused by salt were unexpected. It was also observed that an increase in salt concentration also yields an increase in DNA cleavage when irradiated in 350 nm light.

Compound **2** showed inhibition of photocleavage with the addition of single salts and no enhancement with both salts. For most other DNA photosensitizers, photocleavage yields are decreased due to the condensation of DNA by the salt or the competition by salt for binding sites on the DNA [12]. Spectroscopic analysis of **1** increasing concentration of CT DNA indicated intercalation of this compound with and without the addition of salt. The DNA melting experiments with the addition of the bis-anthracene dye yielded a much higher ΔT_m than the mono-anthracene. Such high T_m values are usually characteristic of a strong binding affinity which is observed in intercalation [38].

Based on photocleavage and UV-visible results by the Grant research group, it can concluded that external binding mode induced by the addition of salt leads to an increase in DNA photocleavage as observed in the case of compound **4**. If the addition of salt produces groove binding, there will be an inhibition of photocleavage as seen in experiments with compound **2**.

5 References

(1) Strekowski, L.; Wilson, B., Noncovalent interactions with DNA: An overview. *Mutat. Res., Fundam. Mol. Mech. Mutagen.* **2007,** *623* (1-2), 3-13.

(2) Haung, Z.; Xu, H.; Meyers, A. D.; Musani, A. I.; Wang, L.; Tagg, R.; Barqawi, A. B.; Chen, Y. K., Photodynamic therapy for treatment of solid tumors-potent - potential and technical challenges. *Technol Cancer Res Treat* **2008 August,** *7* (4), 309-320.

(3) Moan, J.; Peng, Q., An outline of the history of PDT. In *Photodynamic Therapy*, Patrice, T., Ed. The Royal Society of Chemistry: 2003; Vol. 2, pp 1-18.

(4) Gasparro, F. P.; Chan, G.; Edelson, R. L., Phototherapy and photopharmacology. *Yale J. Biol. Med.; Vol. 6* **1985**, Pages: 519-534.

(5) Manyak, M.; Russo, A.; Smith, P.; Glatstein, E., Photodynamic therapy. *Journal of Clinical Oncology* **1988,** *6* (2), 380-391.

(6) Fields, E. J. DNA Photocleavage by Acridine and Phenazine-Based Chromophores. Georgia State University, Atlanta, 2006.

(7) Moan, J., Porphyrin-sensitized photodynamic inactivation of cells: A review. *Lasers in Medical Science* **1986,** *1* (1), 5-12.

(8) Bruce, R. A., Evaluation of hematoporphyrin photoradiation therapy to treat choroidal melanomas. *Lasers Surg. Med.* **1984,** *4* (1), 59-64.

(9) Sigma-Aldrich Hematoporphyrin dihydrochloride. http://www.sigmaaldrich.com/catalog/ProductDetail.do?D7=0&N5=SEARCH_CONCAT_PNO|BRAND_KEY&N4=51250|FLUKA&N25=0&QS=ON&F=SPEC.

(10) Donnelly, R. F.; McCarron, P. A.; Woolfson, D., Drug Delivery Systems for Photodynamic Therapy. *Recent Patents on Drug Delivery and Formulation* **2009,** *3* (1), 1-7.

(11) Allison, R. R.; Sibata, C. H., Oncologic photodynamic therapy photosensitizers: A clinical review. *Photodiagn. Photodyn. Ther.* **2010,** *7* (2), 61-75.

(12) Wilson, B. Syntheses and DNA Interactions of Acridine and Phenothiazine Based Photosensitizers. Georgia State University, Atlanta, 2006.

(13) Cao, H.; Wang, Y., Quantification of oxidative single-base and intrastrand cross-link lesions in unmethylated and CpG-methylated DNA induced by Fenton-type reagents. *Nucleic Acids Res.* **2007,** *35* (14), 4833-4844.

(14) Cooke, M. S.; Evans, M. D.; Dizdaroglu, M.; Lunec, J., Oxidative DNA damage: mechanisms, mutation, and disease. *FASEB J.* **2003,** *17* (10), 1195-1214.

(15) Cadet, J.; Teoule, R., Comparative Study of Oxidation of Nucleic Acid Components by Hydroxyl Radicals, Singlet Oxygen and Superoxide Anion Radicals. *Photochem. Photobiol.* **1978,** *28* (4-5), 661-665.

(16) Blazek, E. R.; Peak, J. G.; Peak, M. J., Singlet Oxygen Induces Frank Strand Breaks as well as Alkali- and Piperidine-Labile Sites in Supercoiled Plasmid DNA. *Photochem. Photobiol.* **1989,** *49* (5), 607-613.

(17) Invitrogen Nucleic Acid Stains. http://www.invitrogen.com/site/us/en/home/References/Molecular-Probes-The-Handbook/Nucleic-Acid-Detection-and-Genomics-Technology/Nucleic-Acid-Stains.html (accessed 02 April 2011).

(18) Blackburn, G. M.; Gait, M. J., *Nucleic Acids in Chemistry and Biology*. 3 ed.; Oxford: New York, 2007.

(19) Kumar, C. V.; Punzalan, E. H. A.; Tan, W. B., Adenine-Thymine Base Pair Recognition by an Anthryl Probe from the DNA Minor Groove. *Tetrahedron* **2000,** *56* (36), 7027-7040.

(20) Kumar, C. V.; Asuncion, E. H., DNA binding studies and site selective fluorescence sensitization of an anthryl probe. *J. Am. Chem. Soc.* **1993,** *115* (19), 8547-8553.

(21) Grant, K. B.; Terry, C. A.; Gude, L.; Fernández, M.-J.; Lorente, A., Synthesis and DNA photocleavage by a pyridine-linked bis-acridine chromophore in the presence of copper(II): Ionic strength effects. *Bioorg. Med. Chem. Lett.* **2011,** *21* (3), 1047-1051.

(22) Wilson, W. D., DNA Intercalators. In *Comprehensive Natural Products Chemistry*, Otto, M.-C.; Sir Derek, B.; Koji, N., Eds. Pergamon: Oxford, 1999; pp 427-476.

(23) Fox, K. R., *Drug-DNA Interactions Protocols*. Humana Press: Totowa, NJ, 1997; Vol. 90.

(24) Neidle, S., Principles of Small Molecule-DNA Recognition. In *Principles of Nucleic Acid Structure*, Academic Press: New York, 2008; pp 132-203.

(25) Martín, B.; Vaquero, A.; Priebe, W.; José, P., Bisanthracycline WP631 inhibits basal and Sp1-activated transcription initiation in vitro. *Nucleic Acids Res.* **1999,** *27* (17), 3402-3409.

(26) Tan, W. B.; Bhambhani, A.; Duff, M. R.; Rodger, A.; Kumar, C. V., Spectroscopic Identification of Binding Modes of Anthracene Probes and DNA Sequence Recognition†. *Photochem. Photobiol.* **2006,** *82* (1), 20-30.

(27) Tuveson, R. W.; Wang, G.-R.; Wang, T. P.; Kagan, J., Light-Dependent Cytotoxic Reactions of Anthracene. *Photochem. Photobiol.* **1990,** *52* (5), 993-1002.

(28) Long, E. C.; Barton, J. K., On demonstrating DNA intercalation. *Acc. Chem. Res.* **1990,** *23* (9), 271-273.

(29) Bast, R. C.; Holland, J. F.; Frei, E.; Society, A. C., *Cancer medicine*. 6th Edition ed.; B.C. Decker: 2000.

(30) DeVita, V. T.; Lawrence, T. S.; Rosenberg, S. A.; Weinberg, R. A.; DePinho, R. A., *DeVita, Hellman, and Rosenberg's cancer: principles & practice of oncology*. Wolters Kluwer/Lippincott Williams & Wilkins: 2008.

(31) Terry, C. A.; Fernández, M.-J.; Grant, K. B.; Lorente, A., Concentrations of NaCl and KCl Increase DNA Photocleavage by a Bis((dimethylamino)methyl)pyridinyl-Linked 9-Aminomethylanthracene Dye. *Biochemistry* **In preparation**.

(32) Modukuru, N. K.; Snow, K. J.; Perrin, J. B. S.; Bhambhani, A.; Duff, M.; Kumar, C. V., Tuning the DNA binding modes of an anthracene derivative with salt. *J. Photochem. Photobiol. A: Chem.* **2006,** *177* (1), 43-54.

(33) Naora, H.; Naora, H.; Izawa, M.; Allfrey, V. G.; Mirsky, A. E., Some Observations on Differences in Composition between the Nucleus and Cytoplasm of the Frog Oocyte. *Proc. Natl. Acad. Sci. U. S. A.* **1962,** *48* (5), 853-859.

(34) Billett, M. A.; Barry, J. M., Role of Histones in Chromatin Condensation. *Eur. J. Biochem.* **1974,** *49* (3), 477-484.

(35) Hooper, G.; Dick, D. A., Nonuniform distribution of sodium in the rat hepatocyte. *J. Gen. Physiol.* **1976,** *67* (4), 469-474.

(36) Sambrook, J.; Fritsch, E. F.; Maniatis, T., *Molecular cloning: a laboratory manual*. Cold Spring Harbor Laboratory: 1989.

(37) Bag, B.; Bharadwaj, P. K., Perturbation of the PET Process in Fluorophore−Spacer−Receptor Systems through Structural Modification: Transition Metal Induced Fluorescence Enhancement and Selectivity. *J. Phys. Chem. B* **2005,** *109* (10), 4377-4390.

(38) Modukuru, N. K.; Snow, K. J.; Perrin, B. S.; Thota, J.; Kumar, C. V., Contributions of a Long Side Chain to the Binding Affinity of an Anthracene Derivative to DNA. *J. Phys. Chem. B* **2005,** *109* (23), 11810-11818.

(39) Duff, M. R.; Mudhivarthi, V. K.; Kumar, C. V., Rational Design of Anthracene-Based DNA Binders. *J. Phys. Chem. B* **2009,** *113* (6), 1710-1721.

(40) Duff, M. R.; Tan, W. B.; Bhambhani, A.; Perrin, B. S.; Thota, J.; Rodger, A.; Kumar, C. V., Contributions of Hydroxyethyl Groups to the DNA Binding Affinities of Anthracene Probes. *J. Phys. Chem. B* **2006,** *110* (41), 20693-20701.